



# Brain networks for clinical purposes

Claudia Testa claudia.testa@unibo.it

Dipartimento di Fisica e Astronomia Università di Bologna

#### The complex brain

Truly complex systems not only have many elements, but those elements are linked through an intricate web of interactions and connections, typically organized on different levels of scale.

It is these interactions that give rise to novel, often surprising and counterintuitive properties.

Such properties are 'emergent' as they are expressed only at larger scales and are completely absent at smaller scales.

the whole is greater than the sum of its parts, or 'more is different'

Mental and cognitive states are irreducible to the mechanics of the brain's individual elements.

It will be useful shifting emphasis from decomposing the brain, reductively, into smaller and smaller bits towards a stronger focus on the principles that govern its operation as an integrated complex system.

#### The complex brain

Three key ingredients will be central to that quest: the mutually interdependent domains of:

#### connectivity,

dynamics, and information.

Dynamics: brain circuits and systems can produce a wide range of dynamical states, manifesting in ever-changing patterns of activation and coactivity. These states reflect the interplay of structural connections, cellular biophysics, plasticity, neuromodulation, sensory input, and the physical and social environment.

Information: tied to fundamental concepts of entropy and patterns of statistical dependencies between ensembles of neurons. Information arises as connectivity shapes neuronal dynamics. Informational patterns range from synchrony, largely a reflection of redundant signals present across multiple neuronal elements, to much less well understood informational features involving higher order interactions such as synergy.

### The complex brain

#### Connectivity.

Connectivity has already become a core concept in neuroscience.

There is a fundamental distinction between **structural connectivity** (material connections) and **functional connectivity** (statistical dependencies).

The dialogue between structure and function animates much of the brain's complexity.

The Human Connectome Project (<a href="https://www.humanconnectome.org/">https://www.humanconnectome.org/</a>) is a project started in 2009 supported by 16 facilities of the National Institutes of Health devoted to the reconstruction of the virtual map of the whole functional and structural connectivity of the human brain.



#### **Connectivity**

Drawing a complete map of the connectome is essential and necessary, but it is not in itself sufficient to capture or explain the diversity of neural states that enable the richness of behavior or generate the flow of experience. Connectivity does not equal cognition and hence, you are not your connectome.

However, like a scaffold or skeleton, the connectome lends shape to the mind.

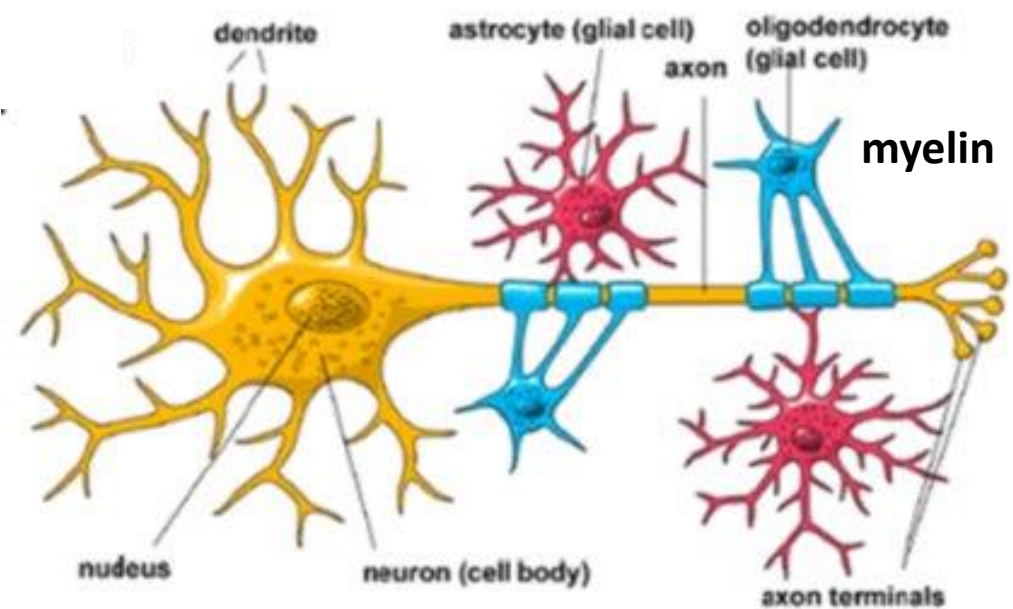
Connectivity defines the space of what is possible, what can be physically realized.

In defining what is possible, connectivity excludes that which is impossible and therefore inacesible to biology and avolution.

Connectivity does not, by itself, explain what brains do, but it firmly rules out what they cannot do.

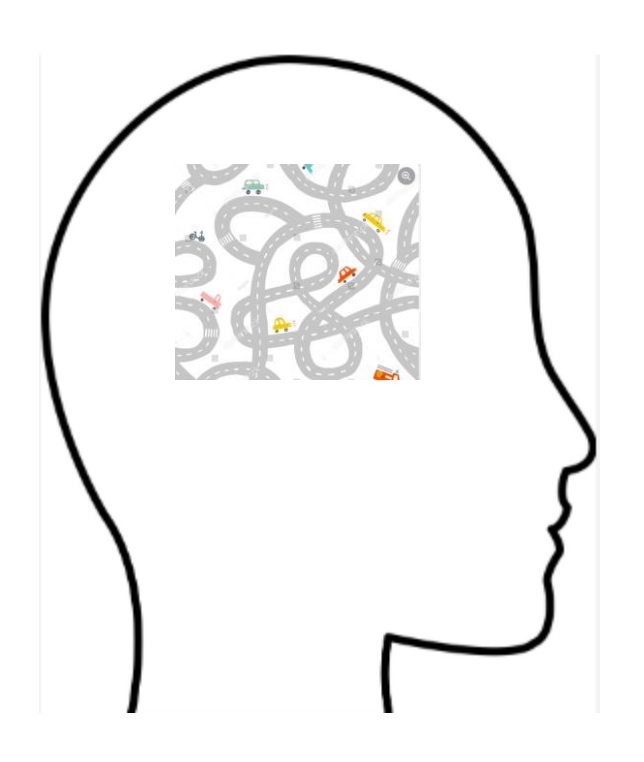
#### **Structural connectivity**

Nerve fibers are covered in myelin, which gives white matter its relatively lighter appearance (hence the name). Myelin insulation increases the information transmission speed of a nerve fiber (i.e., the stuff that keeps the highway of nerve fibers in good condition).



### Water motion to assess the structural connectivity in the brain

Brain contains the nerve fibers of neurons and conducts electrochemical signals to other neurons. These fibers are like *highways* that connect major cities together. When the highways are in better condition, or wider, or more in number, then many cars travel quickly between cities. However, if the highways are in poor condition, or narrower, or fewer in number, then fewer cars can travel and will do so at slower speeds.



# **Diffusion MRI**

Diffusion MRI is a technique that exploits the diffusion of water molecules in brain tissues to generate contrast in MR images.

Signal is given by

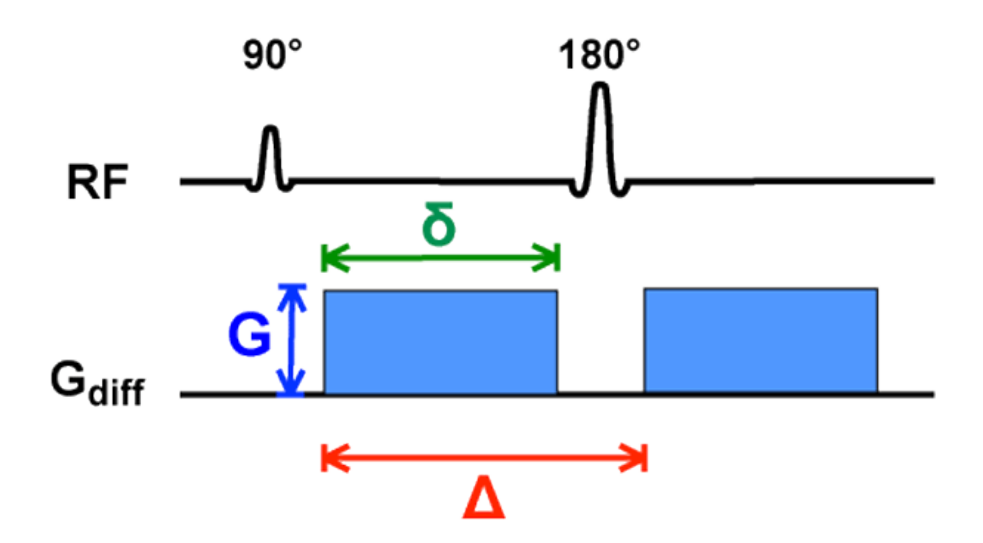
$$S = S_0 \cdot exp(-bD)$$

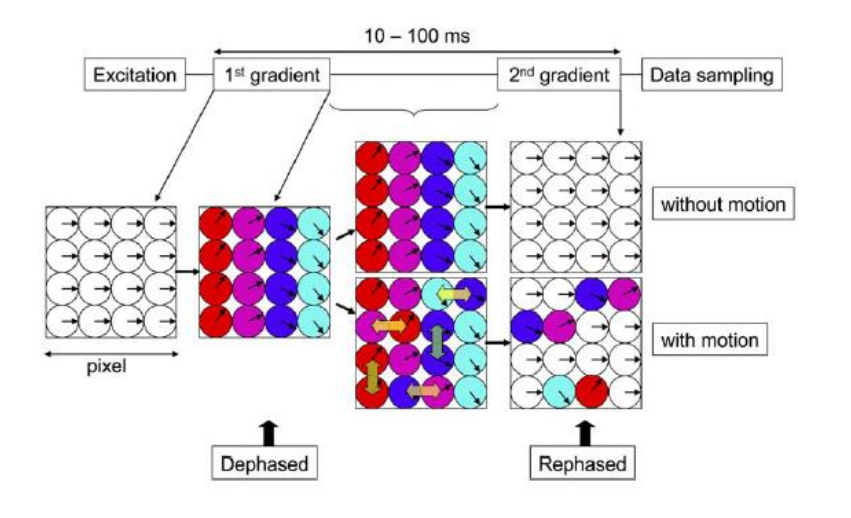
with 
$$b = \gamma^2 G^2 \delta^2 \left( \Delta - \frac{\delta}{3} \right)$$

D is the diffusion coefficient

The 1° gradient after excitation generates a phase shift to signals. During the  $\Delta$  period spins that diffuses acquire an additional phase shift. Thus, the 2° diffusion gradient (equal to the first one) can exactly re-align only those spins that did not diffuse.

Stejskal and Tanner 1965 Pulsed gradient spin-echo sequence



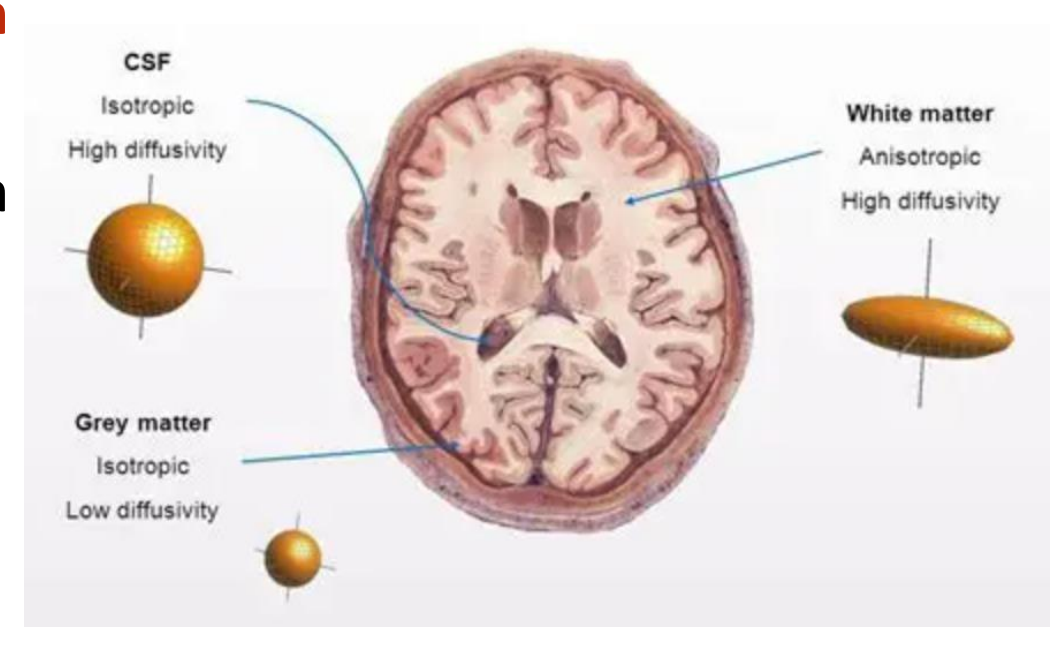


# Isotropic restricted diffusion

Isotropic matter has physical properties that do not depend on the direction of analyis: isotropic matter has the same characteristics in all space directions. CSF in ventricles and grey matter can be semplified as isotropic matter.

### **Anisotropic restricted diffusion**

With anisotropy, physical properties of matter depend on the space direction along with the analysis is run. Physical properties of anistropic matter depend on the direction of analysis.



# **Tractography**

#### What is Tractography?

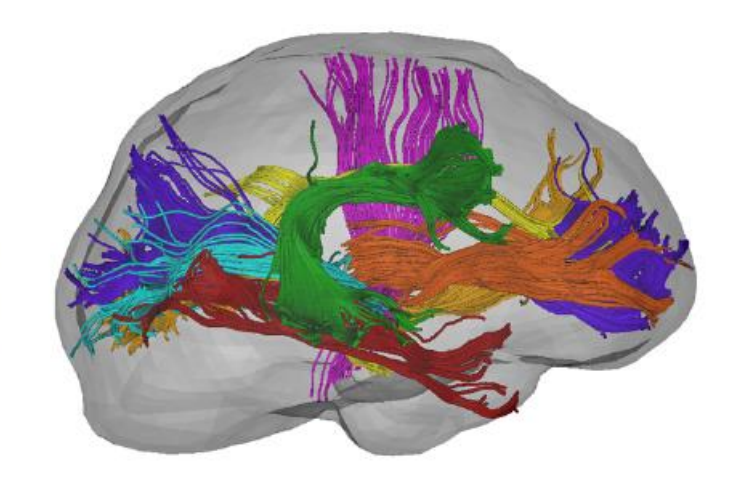




Post-mortem dissection of some white matter fibre bundles (tracts)

#### **Tractography**

The post-imaging reconstruction of fibre bundles/ anatomical connections in the brain using a set of DW images. (in-vivo virtual dissection)



#### **Tractography**

Traces the brain pathways using diffusion data.

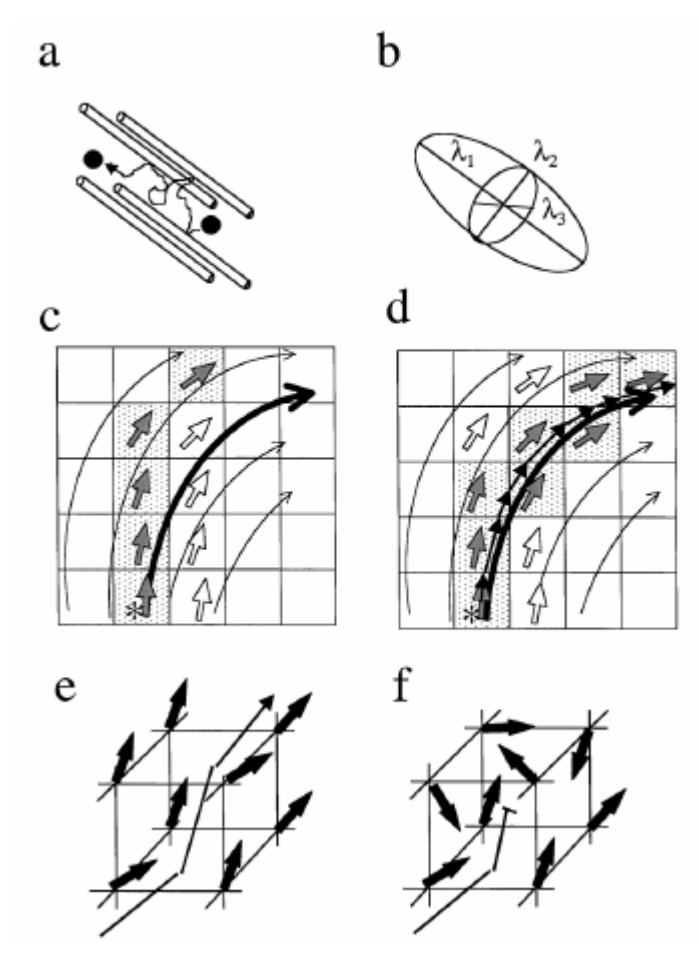
By fitting a diffusion model we can estimate not only mean diffusion and fractional anisotropy but also the orientation of maximum diffusion at each voxel.

Tractography is performed by following these orientation estimates to reconstruct a pathway that, within a coherent bundle, corresponds to the underlying fibre pathway.

Previously, such white matter anatomy could only be studied by post-mortem dissection or invasive tracing in non human animals.

# **Tractography-connectivity**

Assumption: direction of maximum diffusivity in voxels with anisotropic profile is an estimate of the major fibre orientation.



Mori et al Ann of Neurology 1999



Contents lists available at ScienceDirect

#### Magnetic Resonance Imaging

journal homepage: www.elsevier.com/locate/mri



Original contribution

Along-tract analysis of the arcuate fasciculus using the Laplacian operator to evaluate different tractography methods

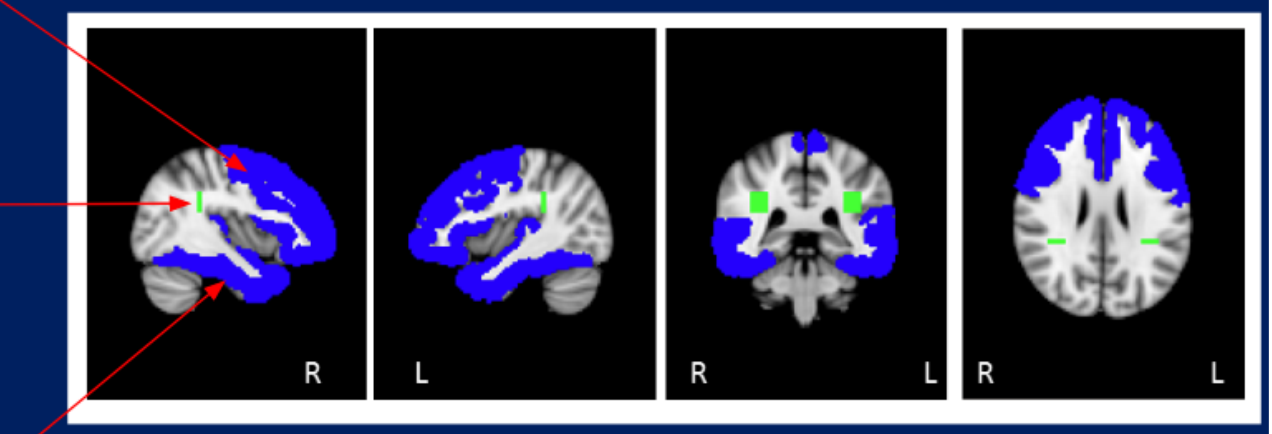


Lia Talozzi<sup>a,1</sup>, Claudia Testa<sup>a,1</sup>, Stefania Evangelisti<sup>a</sup>, Lorenzo Cirignotta<sup>a</sup>, Claudio Bianchini<sup>a</sup>, Stefano Ratti<sup>b</sup>, Paola Fantazzini<sup>c</sup>, Caterina Tonon<sup>a,d,\*</sup>, David Neil Manners<sup>a</sup>, Raffaele Lodi<sup>a,d</sup>

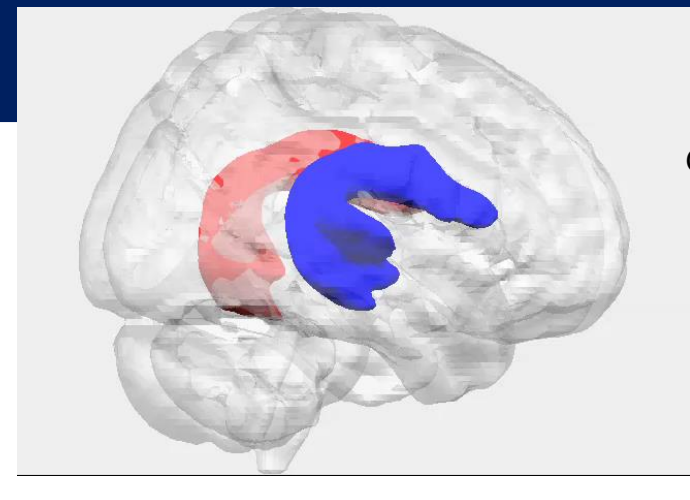
# Along tract analysis with an automatic procedure

#### Target ROI: frontal lobe GM

Seed ROI: WM under the angular gyrus

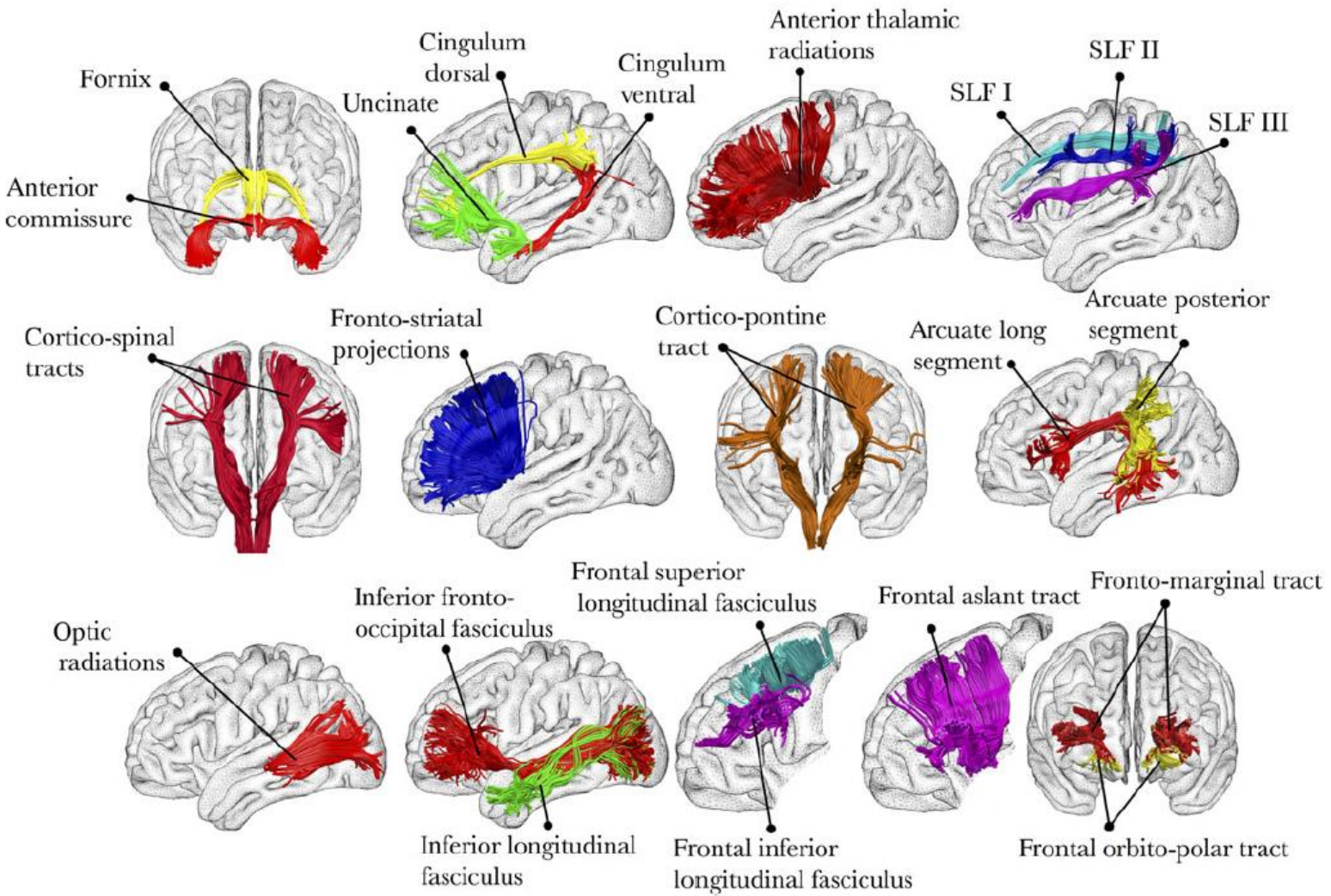


Target ROI: temporal lobe's GM



Giorgio et al., Neuroimage 2010 Galantucci et al., Brain 2011

# **Connectivity – many WM tracts**



Thiebaut de Schotten M, Dell'Acqua F, Ratiu P, et al. From Phineas Gage and Monsieur Leborgne to H.M.: Revisiting Disconnectio n Syndromes. Cereb Cortex. 2015;25(12):4 812-4827.

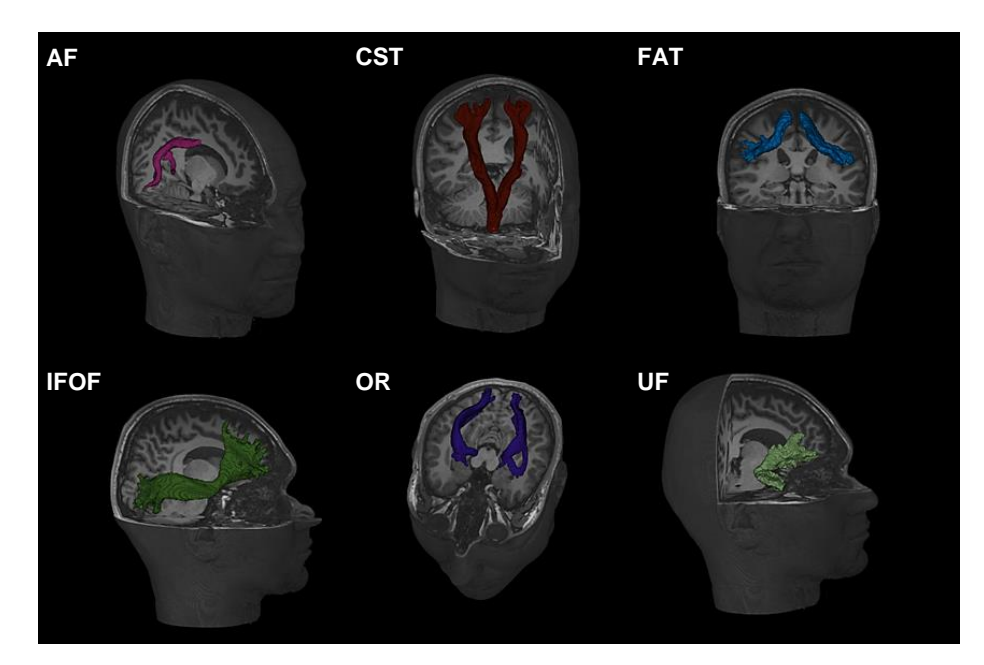
#### Many white matter tracts connectivity

Chack for updates

#### scientific reports

OPEN Assessing robustness
of quantitative susceptibility-based
MRI radiomic features in patients
with multiple sclerosis

Cristiana Fiscono<sup>5,3</sup>, Leonardo Rundo<sup>5,3</sup>, Alessandra Lugaresi<sup>5,3</sup>, David Neil Manners<sup>5,5</sup>,
Kieren Allinson<sup>6</sup>, Eliss Baldin<sup>7</sup>, Gianfranco Vornetti<sup>5,4</sup>, Raffsele Lodi<sup>5,5</sup>, Caterina Tonon<sup>5,6</sup>,
Claudia Tasta<sup>6,6</sup>, Meuro Castelli<sup>7,6,6</sup> & Fulvio Zaccagna <sup>50,13,14,14,14</sup>

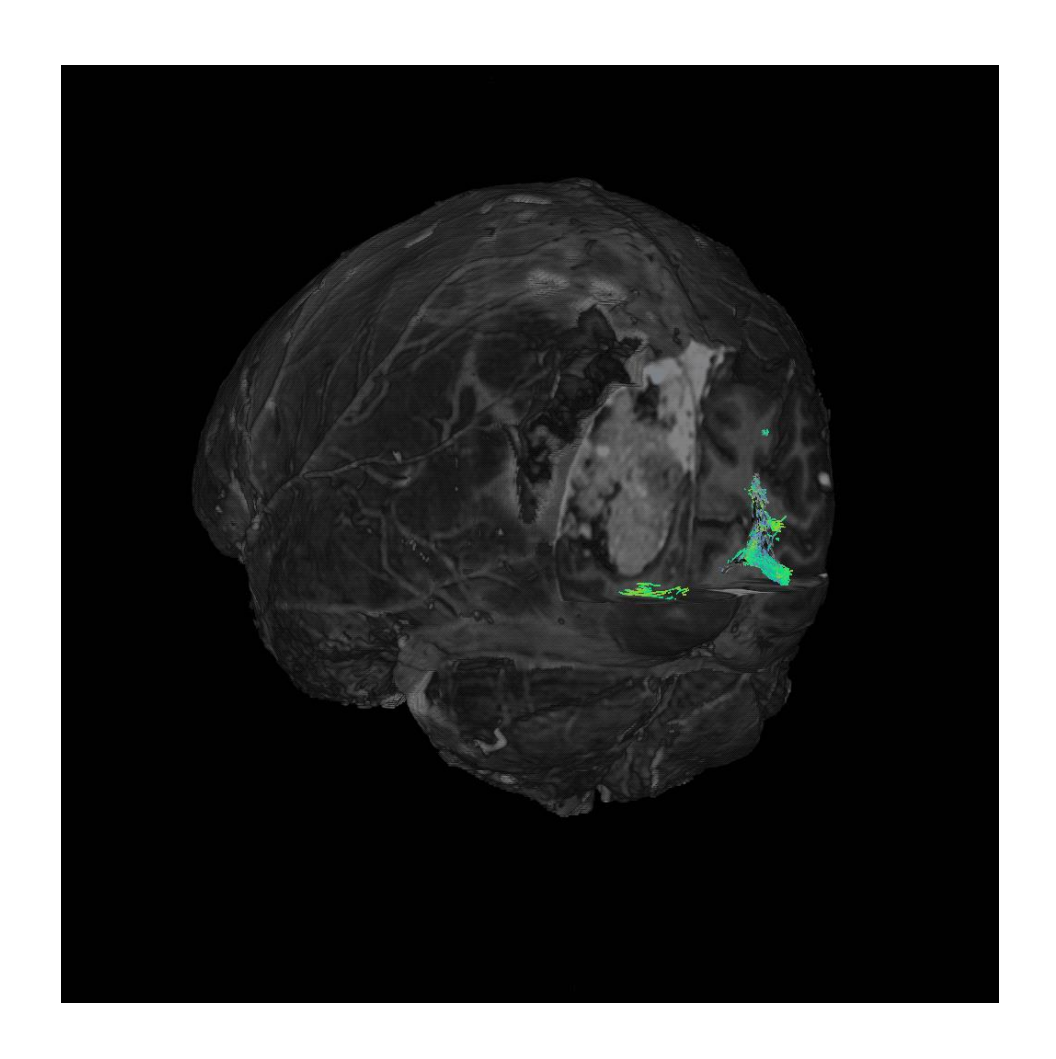


White matter tracts

AF = arcuate fasciculus, CST = cortico-spinal tract, FAT = frontal aslant tract, IFOF = inferior fronto-occipital fasciculus, OR = optic radiation, UF = uncinate fasciculus

## **Neuronal plasticity**

3D reconstruction: it can be visible the structural plasticity of the brain, the optic radiation of the right side is adapted to the presence of the tumor.



#### **Tractography and clinical applications**



ORIGINAL RESEARCH published: 26 February 2021 doi: 10.3389/fneur.2021.633209

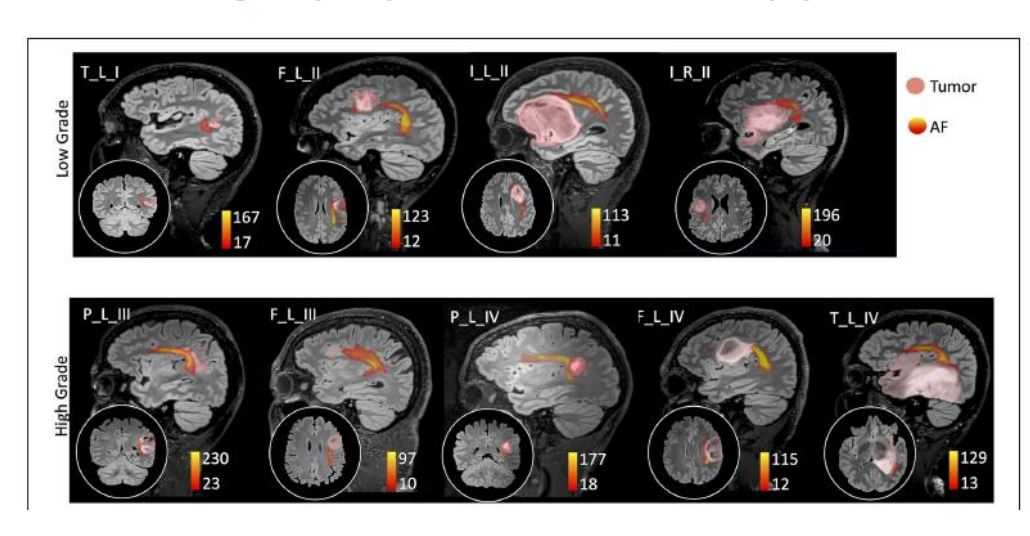


From Neurosurgical Planning to Histopathological Brain Tumor Characterization: Potentialities of Arcuate Fasciculus Along-Tract Diffusion Tensor Imaging Tractography Measures

Matteo Zoli<sup>1,2t</sup>, Lia Talozzi<sup>2t</sup>, Matteo Martinoni<sup>3</sup>, David N. Manners<sup>2</sup>, Filippo Badaloni<sup>3</sup>, Claudia Testa<sup>4</sup>, Sofia Asioli<sup>2,5</sup>, Micaela Mitolo<sup>6</sup>, Fiorina Bartiromo<sup>6</sup>, Magali Jane Rochat<sup>6</sup>, Viscardo Paolo Fabbri<sup>2</sup>, Carmelo Sturiale<sup>3</sup>, Alfredo Conti<sup>2,3</sup>, Raffaele Lodi<sup>2,6</sup>, Diego Mazzatenta <sup>1,2\*t</sup> and Caterina Tonon<sup>2,6‡</sup>

AF tractography allows to detect the course of the tract, favoring the safer-as-possible tumor resection. Our preliminary study shows that along-tract DTI metrics can provide useful information for differentiating LG and HG tumors during pre-surgical tumor characterization.

#### **Tractography and clinical applications**



Sagittal view on the tumor side and coronal or axial focus of the spatial relationship between the tumor (pink colormap) and the arcuate fasciculus (AF)

tractography (colormap red to yellow indicating increasing fiber reconstruction probability). Patients were divided according to low-grade (top panel) and high-grade

(bottom panel) tumors. Patients are labeled according to the tumor's (lobe)\_(hemisphere)\_(grade): frontal (F), temporal (T), parietal (P), and insular (I) lobe; and right (R)

and left (L) hemisphere. For patient P\_L\_IV, a secondary tumor component (light green) is shown within the AF course.

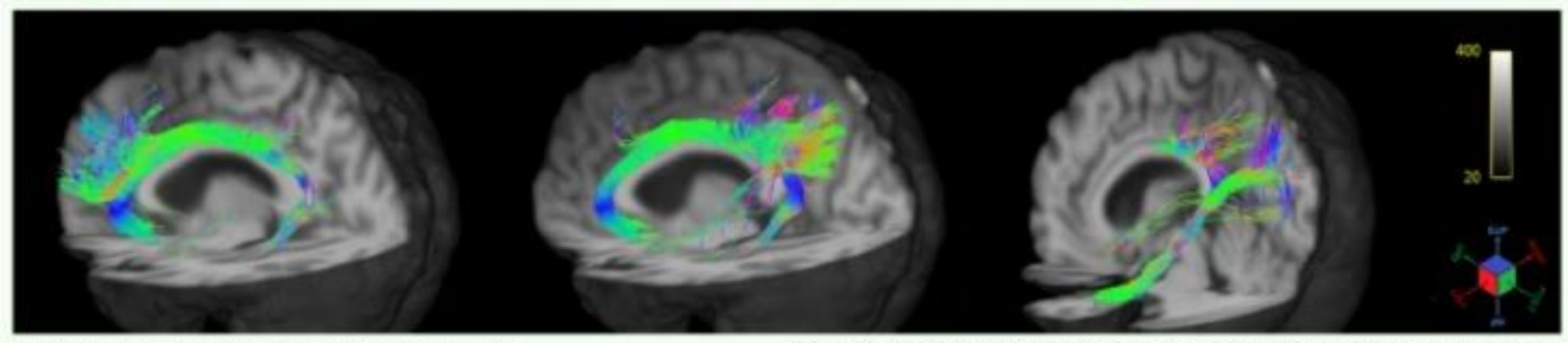
| Measures                | LG tumors<br>Median (min-max)       | HG<br>tumors Median (min-max)       | LG vs. HG p-value | FDR  |  |
|-------------------------|-------------------------------------|-------------------------------------|-------------------|------|--|
| Tumor volume            | 32.9 (4.2–122)                      | 26.4 (13–115.8)                     | 1                 | 1    |  |
| FA # decreased segments | 1.5 (0-4)                           | 6 (2–8)                             | 0.047*            | 0.11 |  |
| Median FA               | 0.43 (0.40-0.45)                    | 0.41 (0.36-0.44)                    | 0.142             | 0.21 |  |
| AD # decreased segments | 1 (1-3)                             | 4 (0-9)                             | 0.306             | 0.37 |  |
| Median AD               | 0.88 (0.77-0.90) mm <sup>2</sup> /s | 0.95 (0.89-0.99) mm <sup>2</sup> /s | 0.027*            | 0.08 |  |
| MD # increased segments | 0 (0-2)                             | 10 (2-14)                           | 0.017*            | 0.07 |  |
| Median MD               | 0.58 (0.56-0.59) mm <sup>2</sup> /s | 0.64 (0.59-0.74) mm <sup>2</sup> /s | 0.014*            | 0.07 |  |
| RD # increased segments | 0 (0-3)                             | 8 (4-10)                            | 0.012*            | 0.07 |  |
| Median RD               | 0.44 (0.43-0.45) mm <sup>2</sup> /s | 0.50 (0.44-0.59) mm <sup>2</sup> /s | 0.086             | 0.17 |  |
| LI fMRI frontal         | 0.30 (0.02-0.86)                    | 0.02 (-0.26 to 0.56)                | 0.221             | 0.29 |  |
| LI fMRI parietal        | 0.37 (-0.20 to 1)                   | -0.18 (-0.62 to 0.18)               | 0.142             | 0.21 |  |
| LI fMRI temporal        | 0.36 (-0.62 to 0.57)                | 0.33 (-0.06 to 0.75)                | 0.806             | 0.88 |  |

\*uncorrected p < 0.05. In bold are comparisons at false discovery rate (FDR) < 0.1.

Non-parametric comparison of lowgrade (LG) and highgrade (HG) tumor patients using Mann-Whitney test, considering tumor volume, along-tract DTI measures [fractional anisotropy (FA), axial diffusivity (AD), mean diffusivity (MD), and radial diffusivity (RD)] median value and number of abnormal AF segments (#) compared with the healthy control (HC) normative distribution, and fMRI laterality index (LI).

# Automatic reconstruction and quantitative measurements of specific bundles

Connectivity related to major brain functions in Alzheimer disease progression: microstructural properties of the cingulum bundle and its subdivision using diffusion-weighted MRI



- The reconstruction of the cingulum bundle is related to major brain functions.
- Its subdivisions exhibit different pathways, terminations, and structural characteristics.
- There are differences in diffusivity metrics among the subdivisions and also between Alzheimer's disease patients and control subjects for some metrics.

3D rendering of the streamlines of the three subdivisions of the cingulum bundle: subgenual (left), the retrosplenial (middle), and parahippocampal (right).

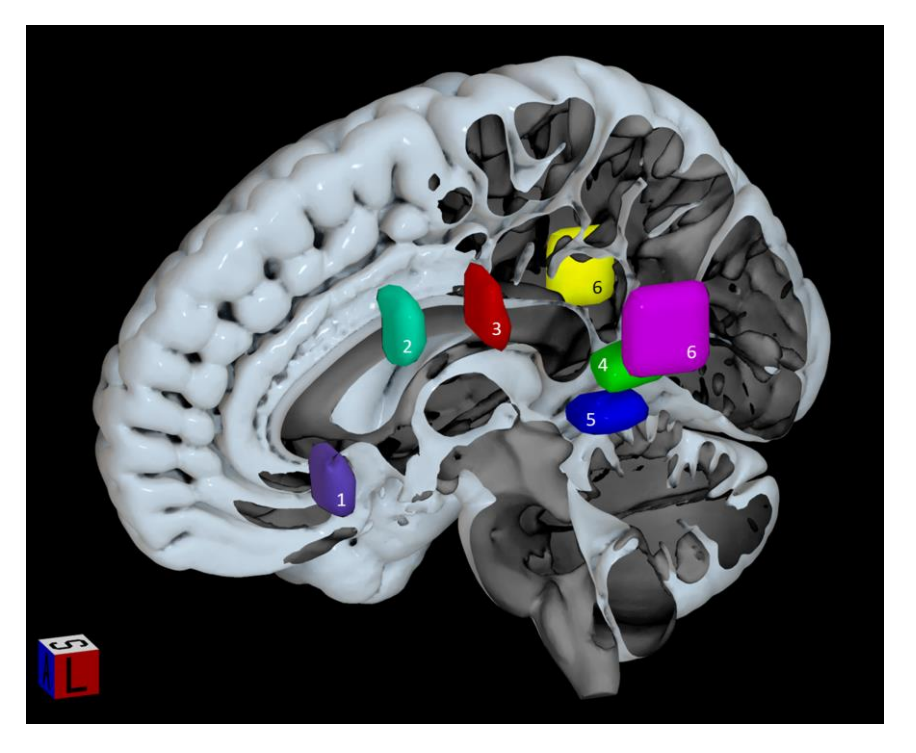
The cingulum bundle is a complex tract with several pathways and terminations related to many functions. We propose a probabilistic automatic approach to reconstruct its subdivisions, showing different microstructural properties and variations with the progression of dementia



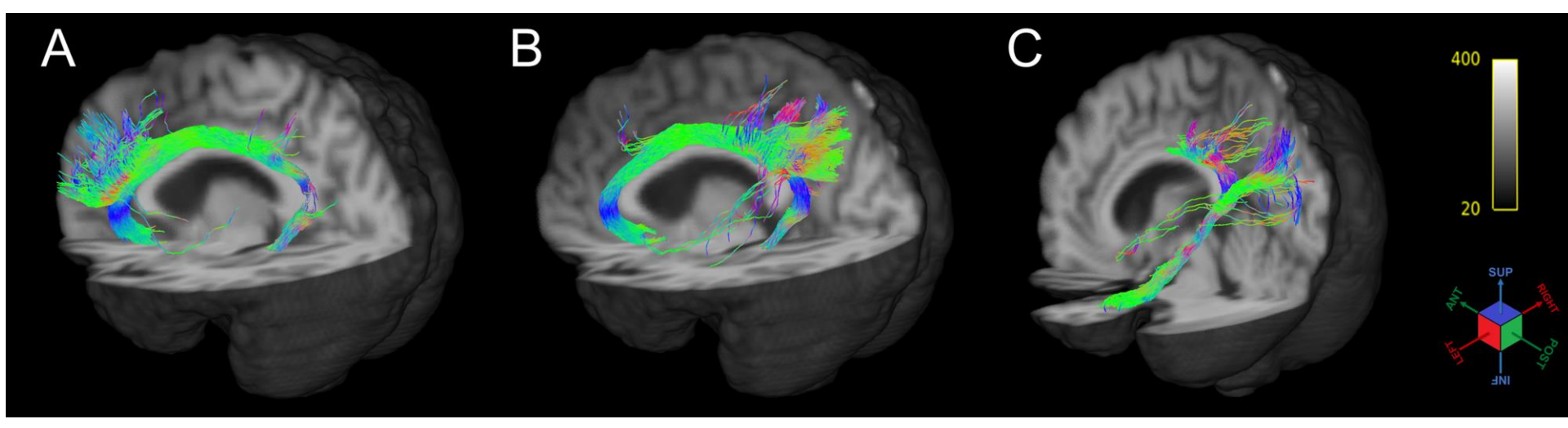
Eur Radiol Exp (2025) Ricchi M, Campani G, Nagmutdinova A et al; DOI: 10.1186/s41747-025-00570-5

# The connectivity related to cognitive functions: microstructural properties of the cingulum bundle and its subdivisions, in the progression of Alzheimer's

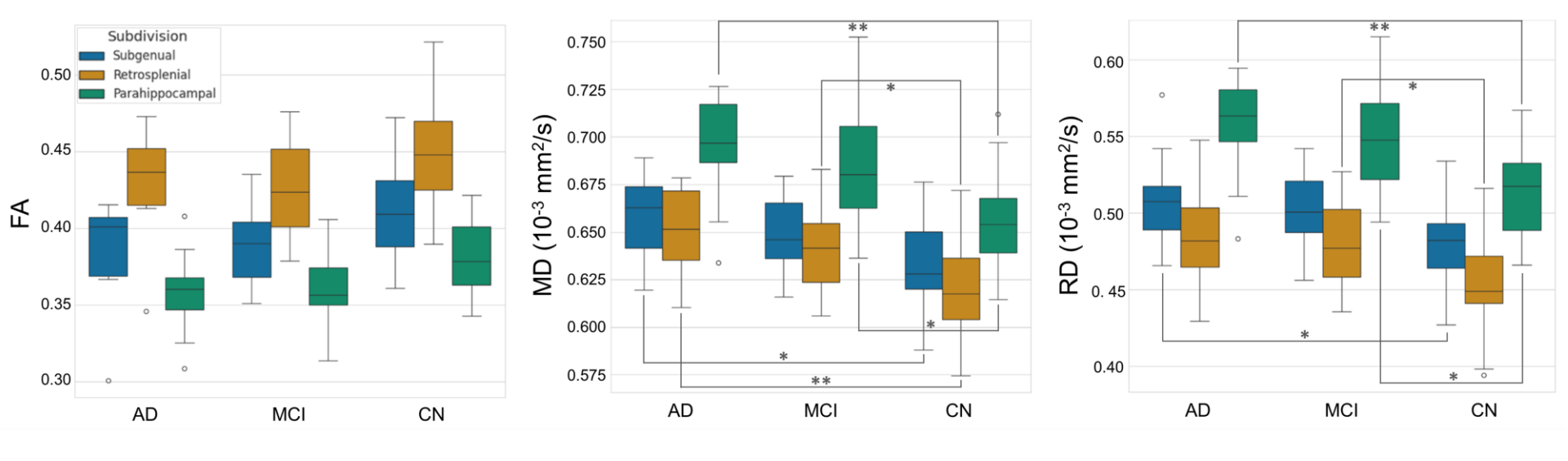
Data: ADNI Initiative (ADNI) database (adni.loni.usc.edu). ADNI was launched in 2003 as a public-private partnership.



ROIs used to reconstruct the three subdivisions of the CB superimposed in the MNI space represented as a surface. ROI 1 (violet) and ROI 2 (teal) were used for the reconstruction of the subgenual subdivision as seed and "include" respectively; ROI 3 (red) and ROI 4 (green) were used for the reconstruction of the retrosplenial subdivision as seed and "include" respectively; ROI 5 (blu), ROI 6 (pink for the left hemisphere and yellow for the right hemisphere) and ROI 4 were used to reconstruct the parahippocampal subdivision as seed, exclude and include respectively.



Three-dimensional rendering of the streamlines of the three subdivisions of the CB for one middle-aged CN case (F, 53 y). In A the subgenual subdivision without the application of the mask; in B the retrosplenial subdivision without the application of the mask; in C the parahippocampal subdivision without the application of the mask (streamlines that may be false positive findings are visible as isolated fibers).



Box-plots of the distribution FA, MD and RD values for the three subdivisions and the three groups of subjects. \* indicates significant differences with a p value<0.05; \*\* indicates significant differences with a p value<0.01.

#### Whole brain Connectomics

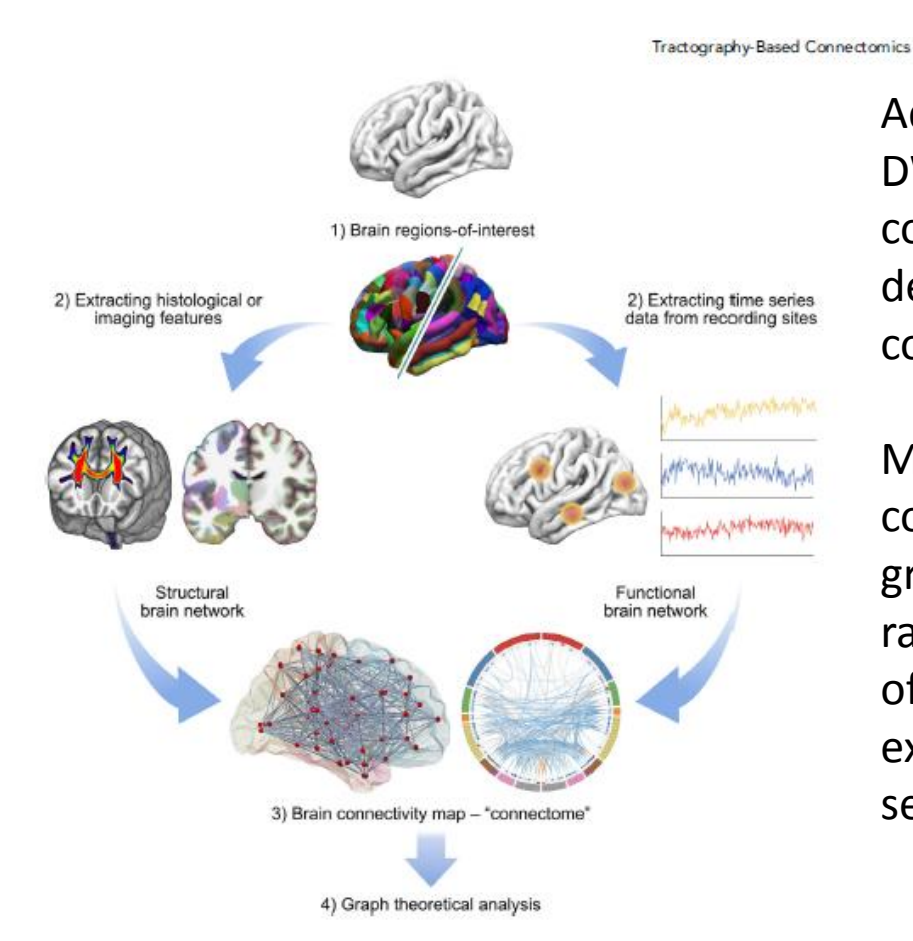
The study of the organization of the connectome, i.e., a (possibly) complete map of the whole connections within the brain.

An increasing number of theoretical and empirical studies approach the brain connectivity from a network perspective by relying on graph theory

Within the domain of human brain mapping, the functional connectivity or functional networks have been constructed from functional MRI (fMRI), electroencephalography (EEG), and magnetoencephalography (MEG), while the anatomical white matter connections or structural networks have been constructed from diffusion tensor imaging (DTI) using computational tractography.



#### Structural Connectomics



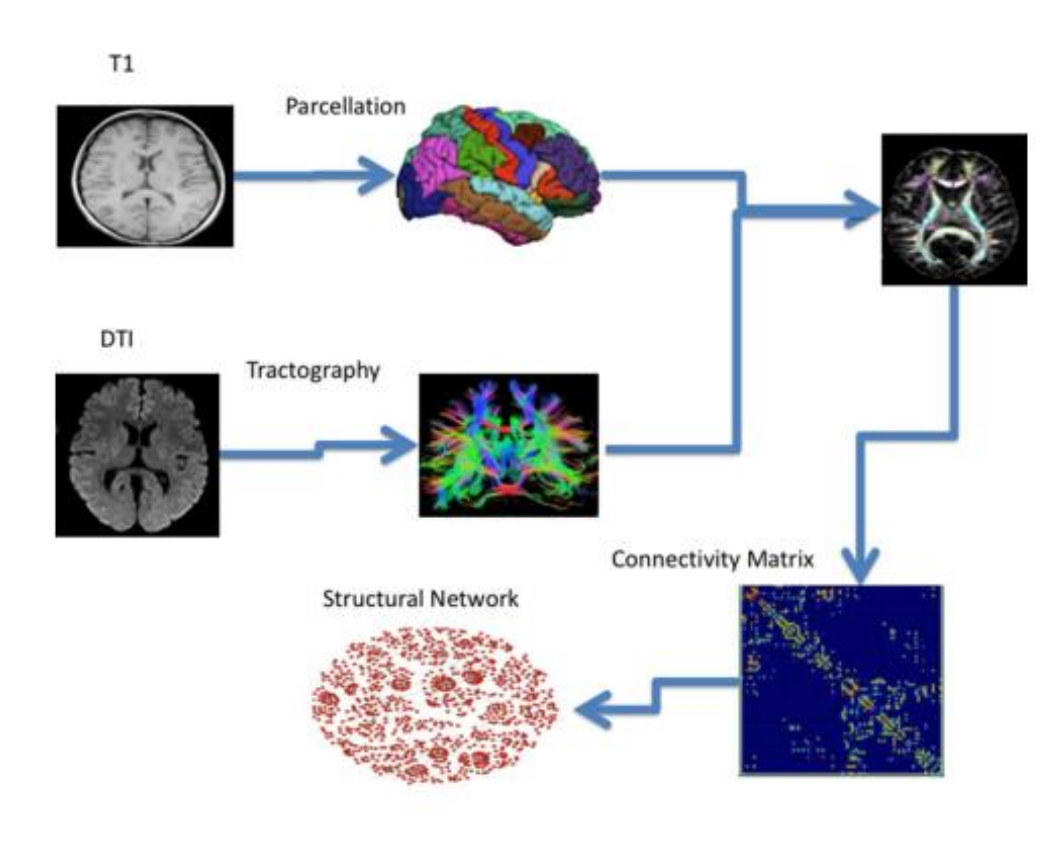
Advanced neuroimaging techniques (fMRI and DWI) have enable identification of the human connectome, i.e., the comprehensive description of brain structural or functional connections.

Much effort toward investigating human brain connectomics focuses on the application of graph theoretical analysis, which provides a range of metrics that characterize the topology of the network. Such metrics facilitate explorations of the information integration, segregation, and propagation in the brain.

Yeh C-H et al. J Mag Res Imaging 2021.



#### **Structural Connectomics**

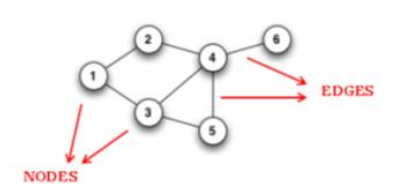


Connectome Construction—focuses on decisions that need to be made in the course of connectome construction.

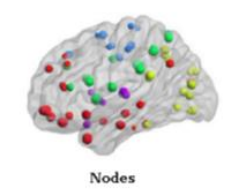
- 1) the choice of a brain parcellation scheme to
- define brain regions-of-interest (ROIs);
- 2) the definition of inter-areal connectivity (Edges);
- 3) the mechanism to associate streamlines with brain GM ROIs

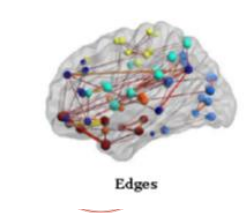
#### **Graph Theory**

A graph is a mathematical structure made by nodes (N) and edges (E) that connect them.









LMA MATER STUDIORUM NIVERSITÀ DI BOLOGNA

#### **Structural Connectomics**

Diffusion MRI data do not provide information about cell bodies or synapses to guide tractography terminations; nevertheless, there are still some fundamental assumptions we could make regarding the required characteristics of any estimated streamline connections generated from the data.

For example: a) fibers should reach at least the interface of GM and WM at both ends;

- b) fibers do not terminate either in the middle of WM or in CSF.
- c) network nodes are typically obtained from brain parcellation of anatomical MRI data.
- d) the connectivity or edge can be defined by the number, length, volume, or probability of all streamlines between the corresponding nodes.

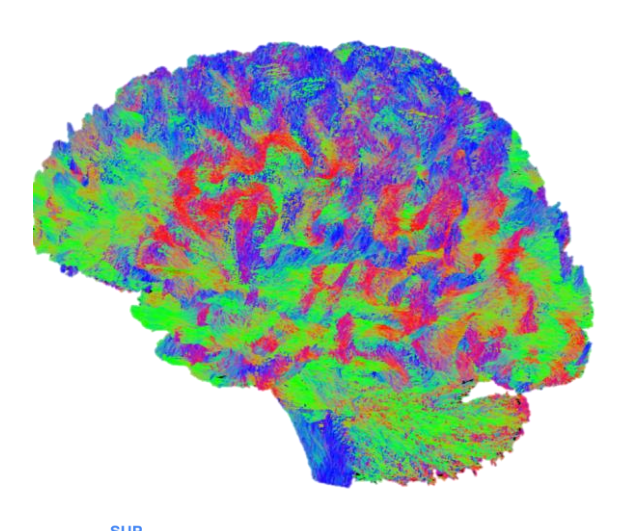
The diffusion metric for the edges can be obtained from the diffusion tensor model (e. g., apparent diffusion coefficient, fractional anisotropy, axial and radial diffusivities), or from other models such as NODDI (e.g., using intracellular volume fraction)



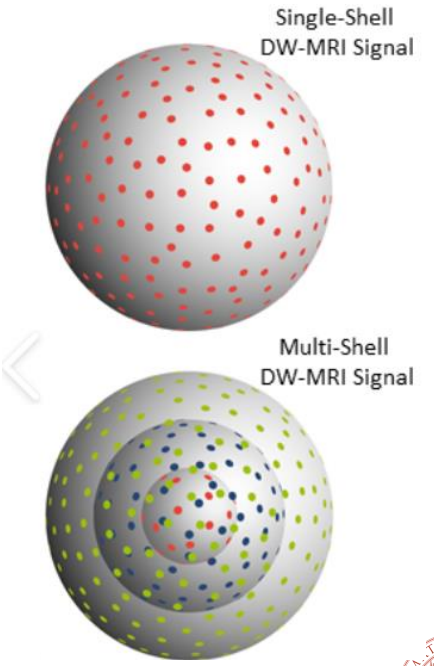
# Validating Microstructure-Weighted Connectomes: A preliminary study on protocol consistency and network metric stability

Cavallo M, Ricchi M, Axford A, Yeung K, McGing J, Brizi L, Tyler DJ, TestaC & Grist JT

In collaboration with Oxford Centre of Magnetic Resonance Submitted to Sci Rep



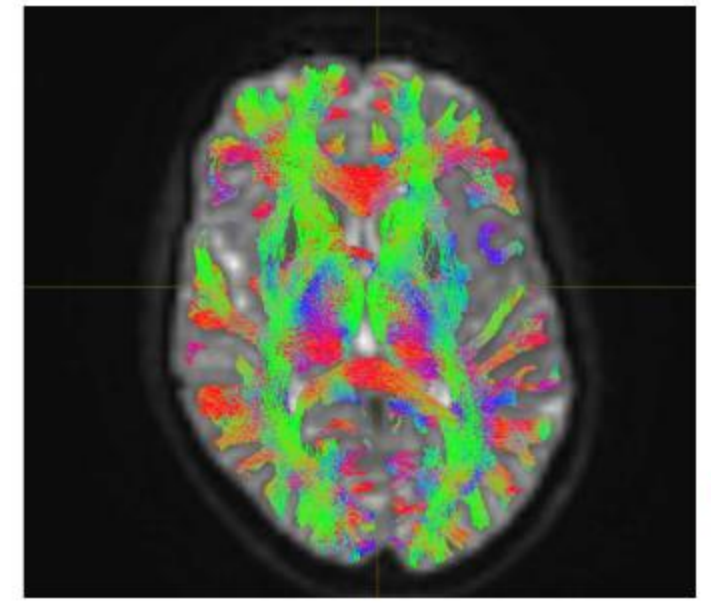
We used a four-shell protocol to apply models for diffusion which introduce several metrics to describe multi compartments of the brain and check the stability of these metrics within patients and repeated measurements.

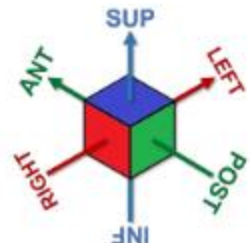




#### Streamline generation

Estimate the fiber trajectories across voxels. These trajectories are called streamlines and are estimates of the underlying white matter tracts, connecting anatomically distinct regions of grey matter. 200k streamlines in the brain of a healthy subject acquired at the University of Oxford. Corpus Callosum correctly has red streamlines as it indicates a left-to-right orientation







#### Weighted connectome

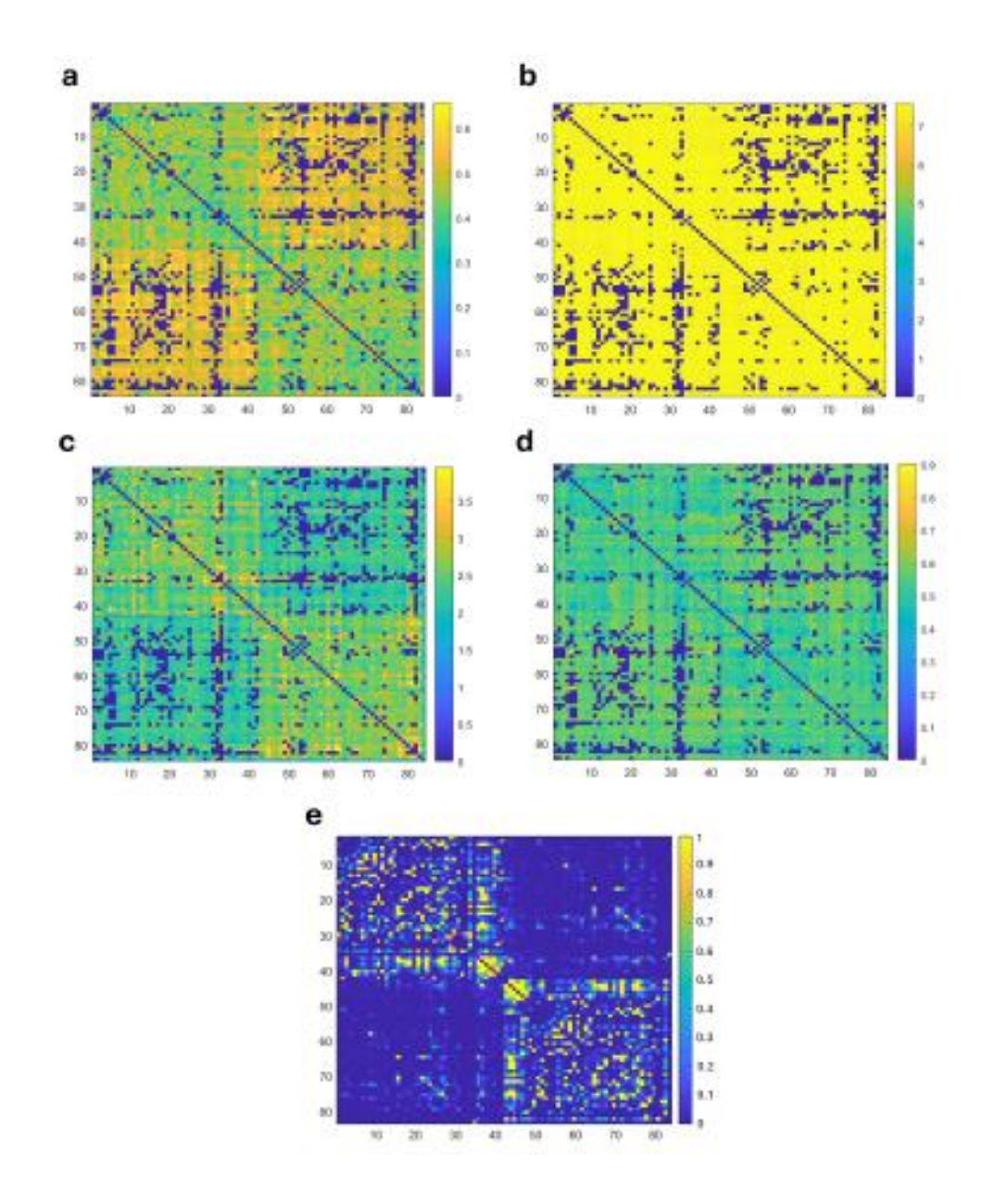
The node parcellation image together with the be used to build the connectome.

The connectome usually represents the strength of the structural connectivity between different regions of the brain i.e. the number of streamlines (NOS) Connecting different parts of the brain.



The connectome can be modelled as a 3D network. Topological properties can be mathematically analyzed by characterizing the brain as an undirected graph, where each region-of-interest composing a greymatter parcellation serves as a node and the edges represents the streamlines between the nodes.





84 × 84 connectome matrices of a healthy volunteer's brain, weighted using:

- a) FA-weighted connectome
- b) MD-weighted connectome
- c) INVF-weighted connectome
- d) ECVF-weighted connectome
- e) NOS-weighted connectome.

|      |                | Density                   |                      | Efficiency                |                      | Modularity                   |                      | Clust. Coeff.        |                      | Mean Strength           |                          |  |
|------|----------------|---------------------------|----------------------|---------------------------|----------------------|------------------------------|----------------------|----------------------|----------------------|-------------------------|--------------------------|--|
|      |                | Site 1 S                  | ite 2                | Site 1                    | Site 2               | Site 1                       | Site 2               | Site 1               | Site 2               | Site 1                  | Site 2                   |  |
| INVF | HV 1           | 0.859 0.<br><b>0.46</b> % |                      | 0.469<br>1.5              |                      | 0.032<br><b>4.9</b> 2        |                      | 0.486<br><b>1.6</b>  | 0.502<br>2%          | 38.900<br>1.55          | 40.124<br>5%             |  |
|      | HV 2           | 0.771 0.785<br>0.90%      |                      | 0.445 0.455<br>1.11%      |                      | 0.057 0.050<br>6.54%         |                      | 0.486 0.493<br>0.72% |                      | 36.917 37.781<br>1.16%  |                          |  |
|      | HV 3           | 0.748 0.784<br>2.35%      |                      | 0.418 0.438<br>2.34%      |                      | 0.089 0.073<br>9.88%         |                      | 0.459 0.471<br>1.29% |                      | 34.673 36.354<br>2.37%  |                          |  |
|      | HV 4           | 0.795 0.822<br>1.67%      |                      | 0.469 0.469<br><b>0</b> % |                      | 0.039 0.039<br><b>9.86</b> % |                      | 0.486 0.501<br>1.52% |                      | 38.900 38.924<br>0.03%  |                          |  |
|      | BA Bias        | -0.021                    |                      | -0.011<br>(-0.026, 0.003) |                      | 0.005                        |                      | -0.013               |                      | -0.948                  |                          |  |
|      | 95% CI         | (-0.043,                  | 0)                   |                           |                      | (-0.011, 0.021)              |                      | (-0.019, -0.006)     |                      | (-2.138, 0.242)         |                          |  |
|      | HV 1           | 0.859 0.<br><b>0.46</b> % |                      | 2.084<br><b>2.9</b> 2     | 2.210<br><b>2</b> %  | 0.077<br><b>0.6</b> 5        |                      | 2.153<br>2.8         | 2.281<br>9%          | 173.004<br><b>2.9</b> 2 | 183.425<br>2%            |  |
| ECVF | HV 2           |                           | 0.771 0.785<br>0.90% |                           | 1.833 2.066<br>5.98% |                              | 0.105 0.101<br>1.94% |                      | 1.993 2.228<br>5.57% |                         | 152.129 171.476<br>5.98% |  |
|      | HV 3           | 0.748 0.<br>2.35%         |                      | 1.795<br><b>3.4</b>       |                      | 0.142<br><b>6.7</b>          | 0.124<br>7%          |                      | 2.066<br>8%          | 149.010<br>3.41         |                          |  |
|      | HV 4           | 0.795 0.822<br>1.67%      |                      | 1.941<br><b>6.4</b>       | 2.207<br>1%          | 0.085<br><b>10.</b> 3        | 0.069<br><b>9%</b>   |                      | 2.355<br><b>7</b> %  | 161.110<br><b>6.4</b> 0 |                          |  |
|      | BA Bias -0.021 |                           |                      | -0.188                    |                      | 0.010                        |                      | -0.174               |                      | -15.585                 |                          |  |
|      | 95% CI         | (-0.043, 0)               |                      | (-0.311, -0.065)          |                      | (-0.005, 0.024)              |                      | (-0.301, -0.046)     |                      | (-25.767, -5.403)       |                          |  |



# **Functional connectivity**

The phatophysiological study of brain diseases has allow to assess that they can be grouped in terms of two fundamental principles of brain organization: functional segregation and integration

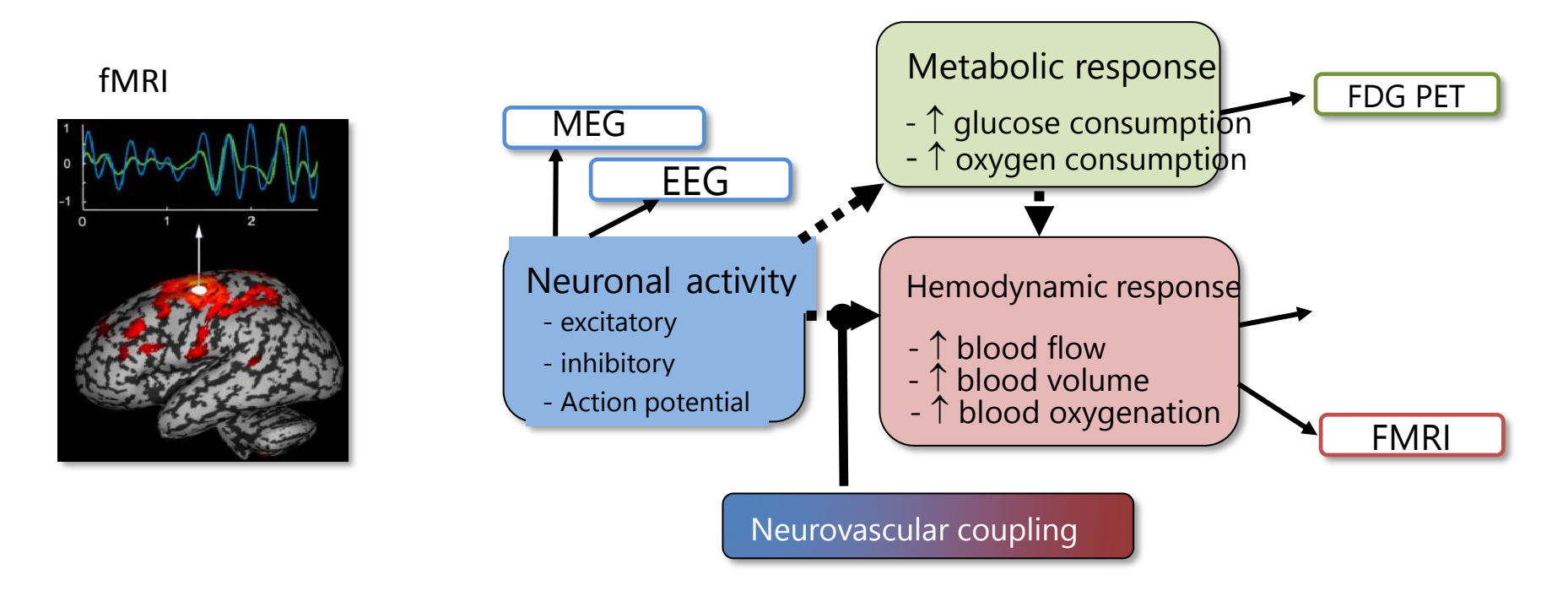
- Functional segregation refers to the specialization of discrete brain regions or systems in performing specific mental operations
- Functional integration is achieved via precise dynamical coordination of these segregated elements and is contingent on intact axonal and synaptic connectivity

Attempts to map the human connectome have used MRI because It provides an efficient, cost-effective and non-invasive means for characterizing structural and functional properties of the entire brain-

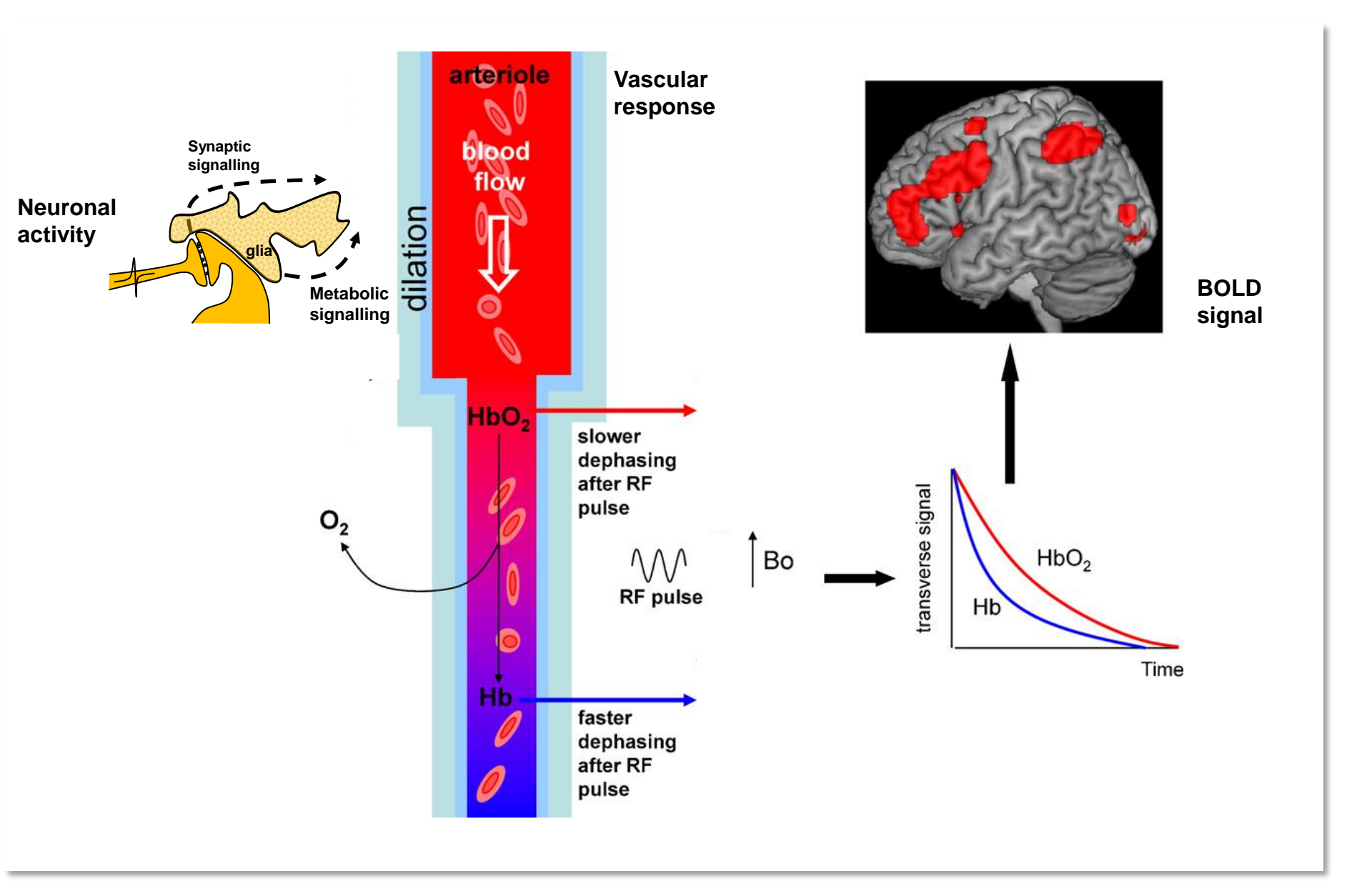
### Functional magnetic resonance imaging (fMRI)

Focus on metabolism and functionality and on connectivity

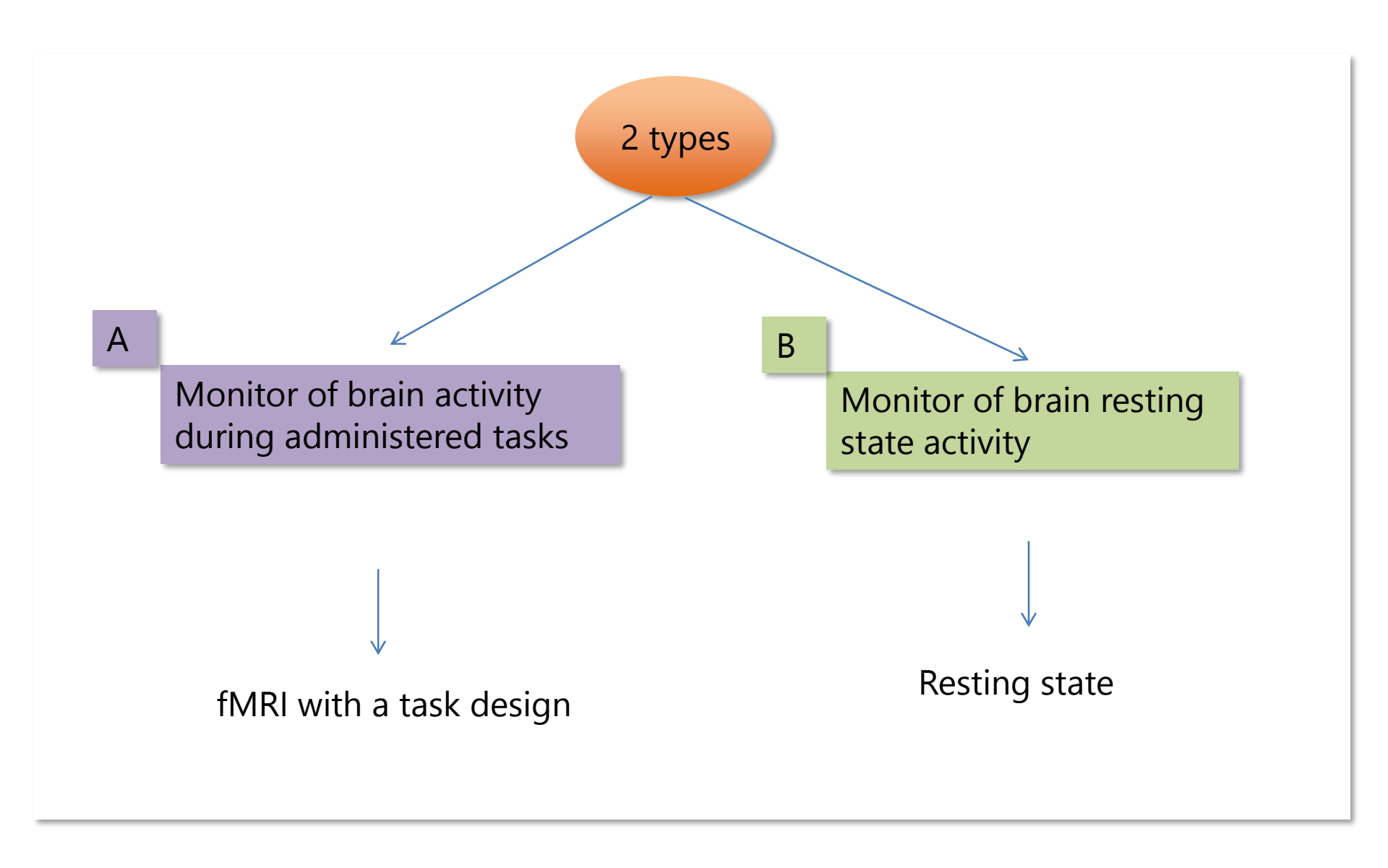
# Investigation of the functional organization of the BRAIN



# From neuronal activity to the fMRI signal



# Design of an fMRI acquisition



# Design of an fMRI acquisition

#### A): Monitor of brain activity during administered tasks

BOLD signal is due to a signal intesity variation of about  $\sim$  5 %; it is very weak to be distinguished by the basal condition.

During acquisition, a paradigm is administered to the subject: *sensory*, *motor* or *cognitive* taks are administered.

The same task is periodically repeated to perform an average of images acquired during the stimuli.

Task periods are alternated with rest periods in which the subject relaxes (basal condition).

-the analysis will compare in average the BOLD signal during task with respect to the rest condition

#### The equipment

- 3T MR scanner (Siemens Magnetom Skyra)
- 64-channel brain phased array coil (Head/Neck 64)



• fMRI NordicNeuroLab Visual System HD



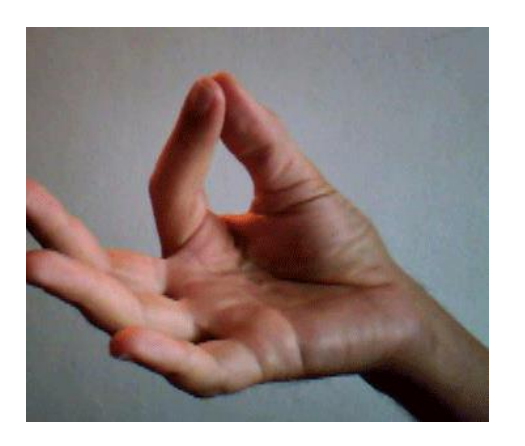
## Clinical application of fMRI for pre-surgical planning

Tumor lesion close to the motor area

#### **MAPPING sensori-motor functions**

- Finger tapping
- Close-open hands
- 3. Lip and tongue movements
- Flex-estension foot





FMRI finger tapping (left hand)

in a patient with a lesion in the right hemisphere

#### **Tractography and fMRI**



ORIGINAL RESEARCH published: 03 June 2022 doi: 10.3389/fneur.2022.867048



Frontiers in Neurology • Article • Open Access • 2022 • DOI: 10.3389/fneur.2022.867048

Mitolo, Micaela<sup>a,b</sup>; Zoli, Matteo<sup>c,d</sup>; Testa, Claudia<sup>a,e</sup>; Morandi, Luca<sup>a,d</sup>; Rochat, Magali Jane<sup>a</sup>; +10 authors

#### Neuroplasticity Mechanisms in Frontal Brain Gliomas: A Preliminary Study

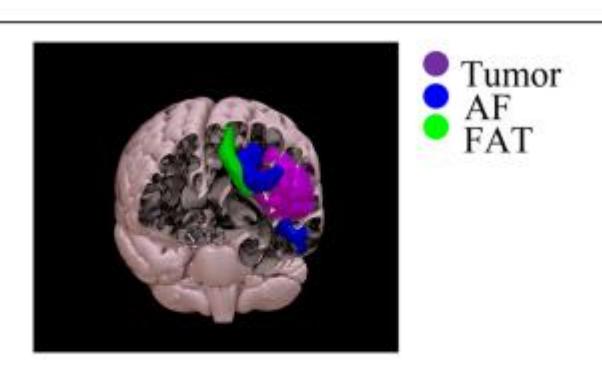


FIGURE 1 | Three-dimensional rendering of the reconstruction of the AF (blue), FAT (green), and tumor segmentation (violet) in the same patient with left frontal glioblastoma grade 4.

The hemispheric laterality index (LI) was calculated through phonemic fluency task functional MRI (fMRI) activations in the frontal, parietal, and temporal lobe Parcellations.

Arcuate Fasciculus (AF) and Frontal Aslant Tract (FAT) tractography was performed using constrained spherical deconvolution diffusivity modeling and probabilistic fiber tracking.

#### **Tractography and fMRI**

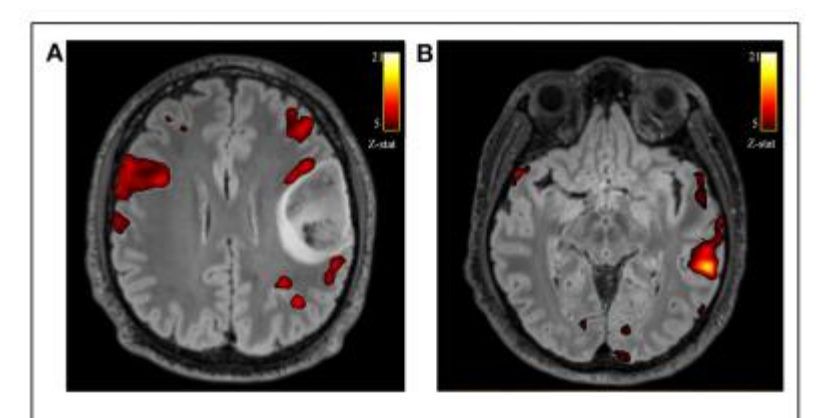


FIGURE 2 | Axial views of the T2-w FLAIR image superimposed the fMRI phonemic fluency fMRI activation. Example of one patient with left frontal glioblastoma grade 4, showing the recruitment of contralateral compensatory activation of right frontal operculum (A) and canonical temporal activation on the left hemisphere (B).

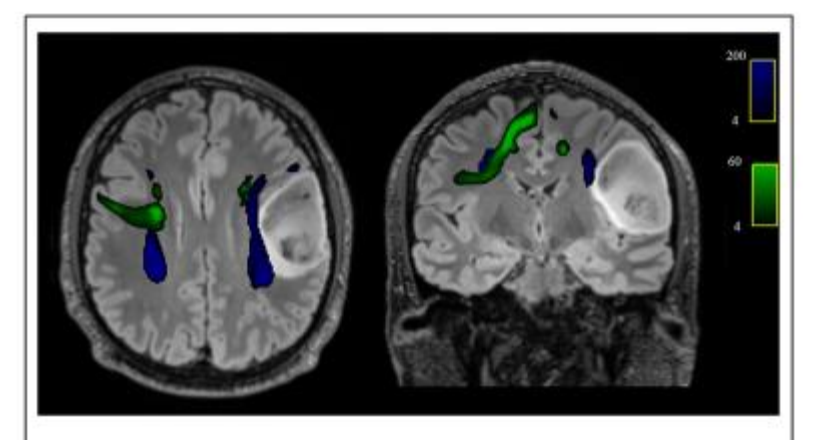


FIGURE 3 | Axial and coronal views of the T2-w FLAIR image with superimposed the reconstruction of the AF (blue) and FAT (green) of one patient with left frontal glioblastoma grade 4, showing the spatial relationship between the tumor and tracts and in particular the displacement of both left AF and FAT.

TABLE 4 | Comparison of DTI parameters between patients and healthy controls.

| DTI features |    | HC (N = 24) |       | LG patients (N = 10) |       | LG patients vs. HC | RG patients ( $N = 5$ ) |       | RG patients vs. HC |  |
|--------------|----|-------------|-------|----------------------|-------|--------------------|-------------------------|-------|--------------------|--|
|              |    | Mean        | Sd    | Mean                 | Sd    | P-value            | Mean                    | Sd    | p-value            |  |
| Left FAT     | MD | 0.594       | 0.020 | 0.637                | 0.072 | 0.021*             | 0.598                   | 0.038 | NS                 |  |
|              | FA | 0.404       | 0.025 | 0.385                | 0.053 | NS                 | 0.404                   | 0.034 | NS                 |  |
| Left AF      | MD | 0.586       | 0.019 | 0.607                | 0.019 | 0.021*             | 0.595                   | 0.030 | NS                 |  |
|              | FA | 0.450       | 0.024 | 0.424                | 0.019 | 0.021*             | 0.427                   | 0.037 | NS                 |  |
| Right FAT    | MD | 0.593       | 0.022 | 0.602                | 0.014 | NS                 | 0.668                   | 0.076 | 0.001*             |  |
|              | FA | 0.405       | 0.023 | 0.389                | 0.027 | NS                 | 0.340                   | 0.050 | NS                 |  |
| Right AF     | MD | 0.586       | 0.020 | 0.589                | 0.016 | NS                 | 0.671                   | 0.106 | 0.027*             |  |
|              | FA | 0.433       | 0.033 | 0.415                | 0.030 | NS                 | 0.385                   | 0.075 | NS                 |  |

Furthermore, patients with low grade tumor, showed higher rightward frontal operculum fMRI activations and better cognitive performance in tests measuring general cognitive abilities, semantic fluency, verbal short-term memory, and executive functions.

## Design of an fMRI acquisition

B): monitor of brain resting state activity

#### Resting state:

The subjects lies without doing anything during the acquisition time. A brain activity is still present because of spontaneous activity at low frequency (<0.1 Hz).

At the origin of this interest there was a debate: How much of this is noise and how much is interesting information?

The first paper: Biswal 1995......

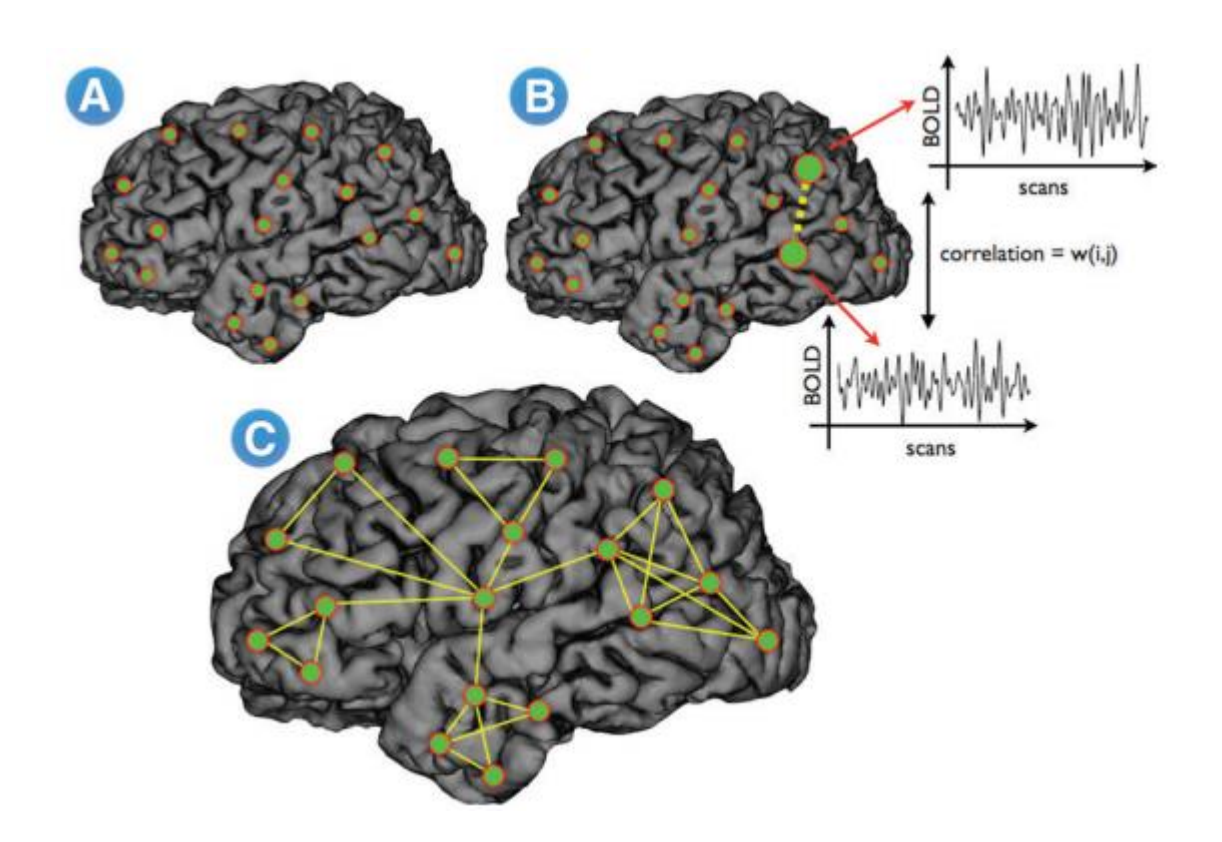
.....and now many papers

### **Functional connectivity**

Functional connectivity:

Network identification, brain areas ensemble, which are connected during the resting state fMRI.

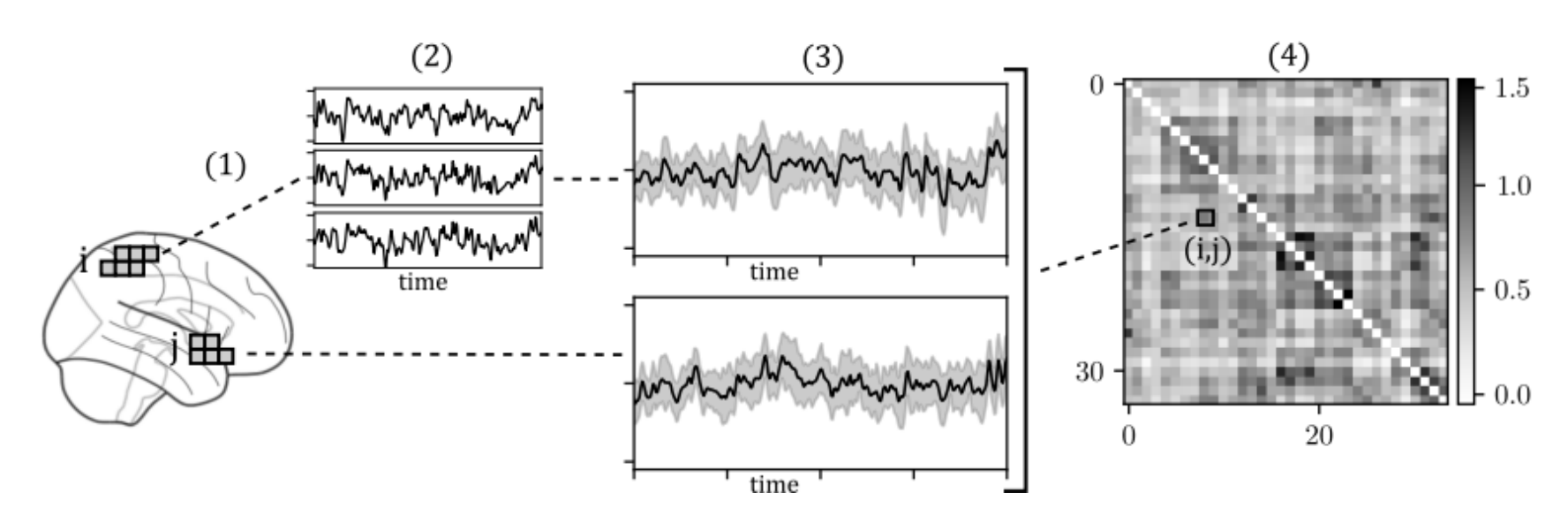
Functional connettivity: «similar» temporal pattern



### **Functional connectivity**

In typical resting state-FMRI the brain is supposed to be in a stationary state ehere distinct brain regions, rather than being totally silent, show weak but coherent (i.e. temoprally similar) low-frequency BOLD signal fluctuations.

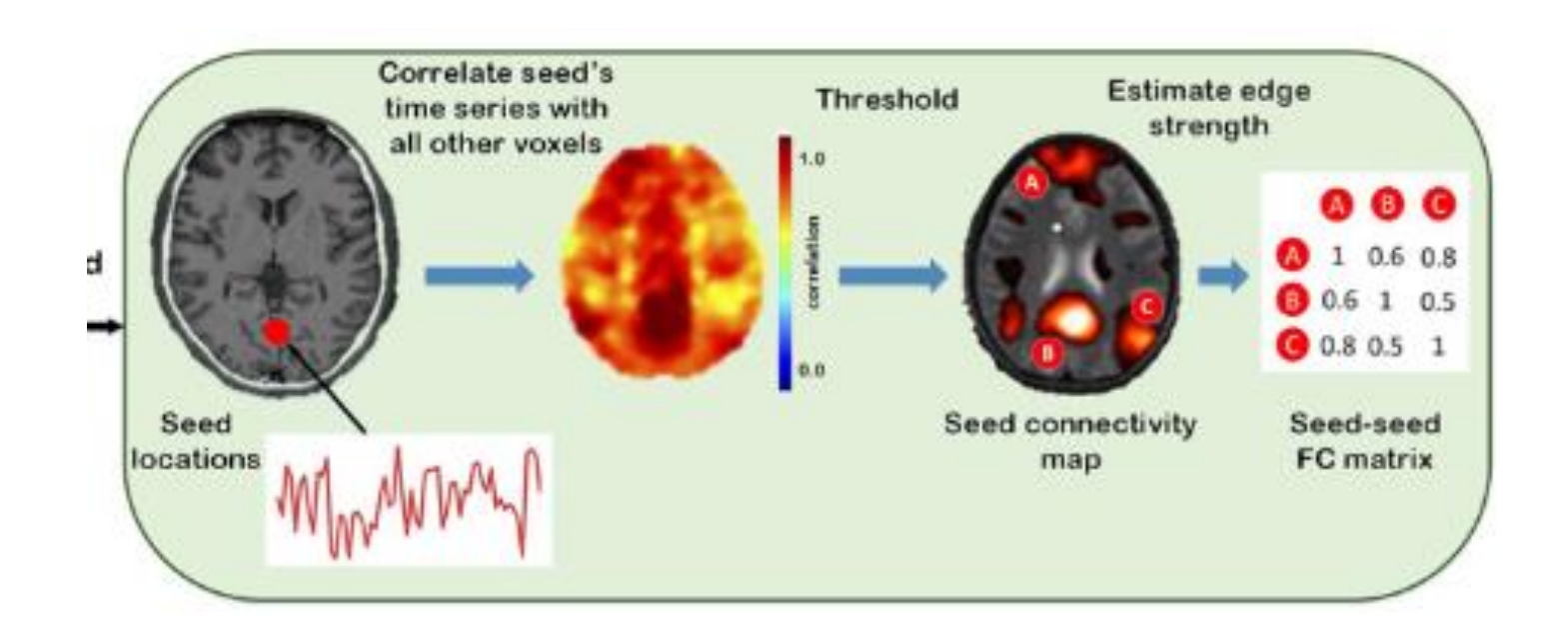
Functional connectivity: similar temporal patterns.



Schematics of the steps required for graph construction: (1) Extraction of single voxels' time series from EPI data; (2) Computing ROIs average time series; (3) Pearson correlation between time series, removing negative correlation values and Z-transformation.

## **Data analysis-resting state**

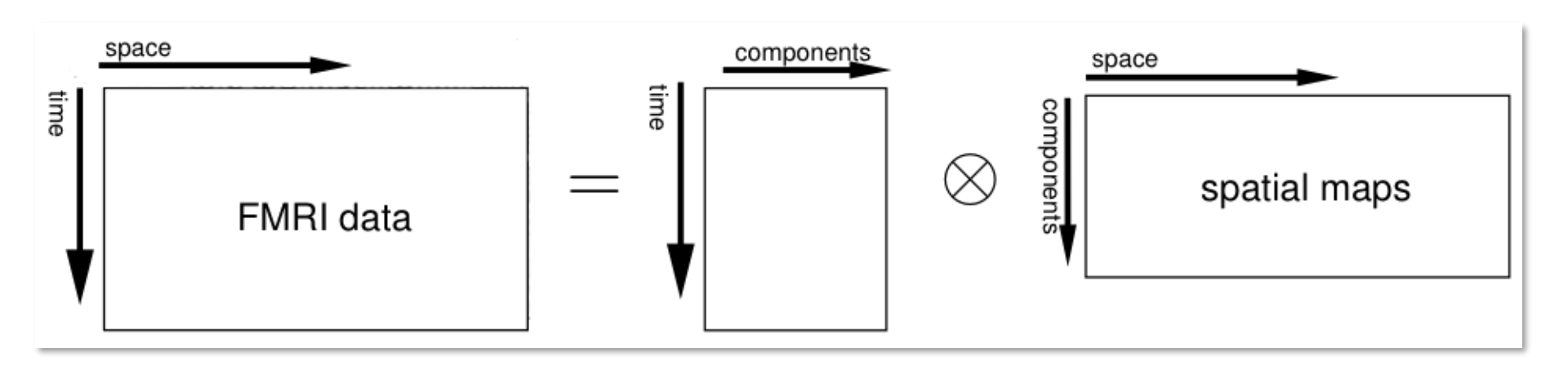
Example: seed-based approach

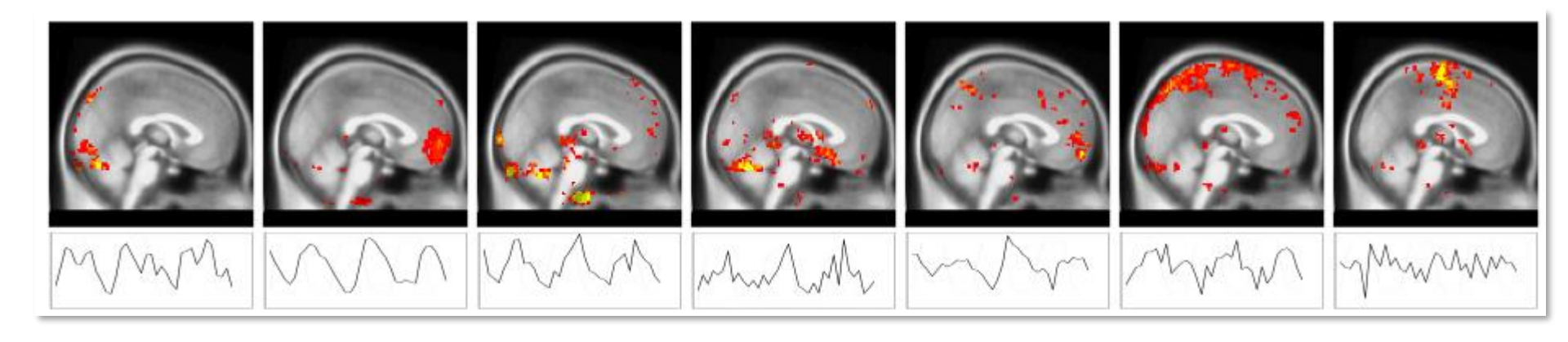


$$\rho_{X,Y} = \frac{\text{cov}(X,Y)}{\sigma_X \sigma_Y}$$

## **Data analysis-resting state**

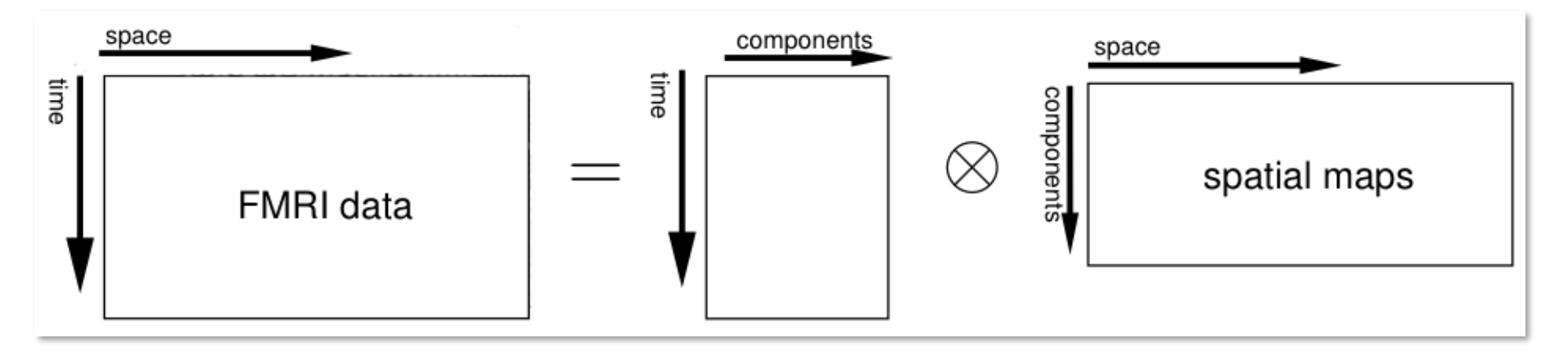
Example: ICA (Independent Component Analysis)





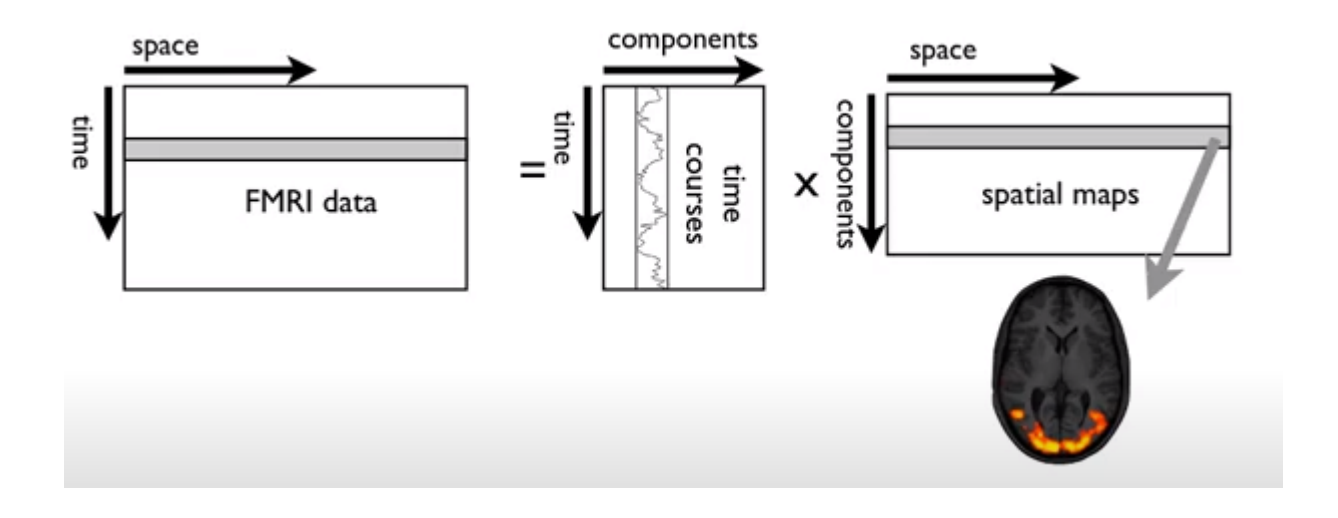
## **Data analysis-resting state**

ICA assumes that fMRI data are a set independent signal components which come from a certain number of sources spatially distributed. ICA decomposes data in these numerous independent components.



- No initial assumption
- A posterior selection of valid components (with a manual/visual approach or with automatical approach)
- Complex group analysis because of the need of the selection of components which are correspondent between different subjects

## **Spatial ICA for fMRI**



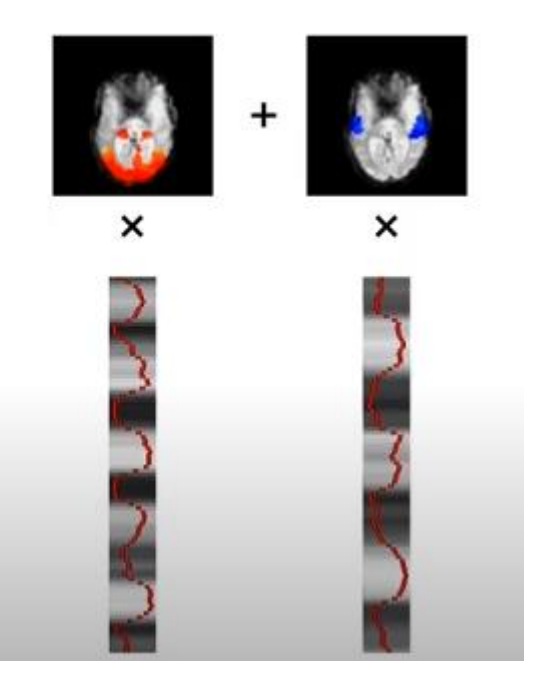
Data is decomposed into a set of spatially independent maps and a set of time-courses———— we are interested in the spatial maps.

## What are components?

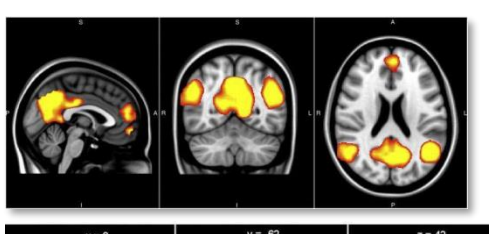
Ex:Data of fMRI with visual and auditory stimuli.



ICA expresses observed data as linear combination of spatio-temporal processes



### **Resting – state networks**



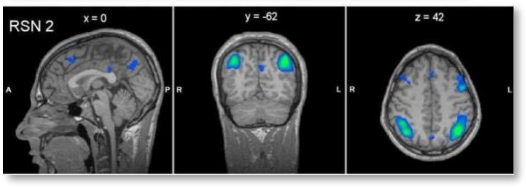
Default mode network

# Consistent resting-state networks across healthy subjects

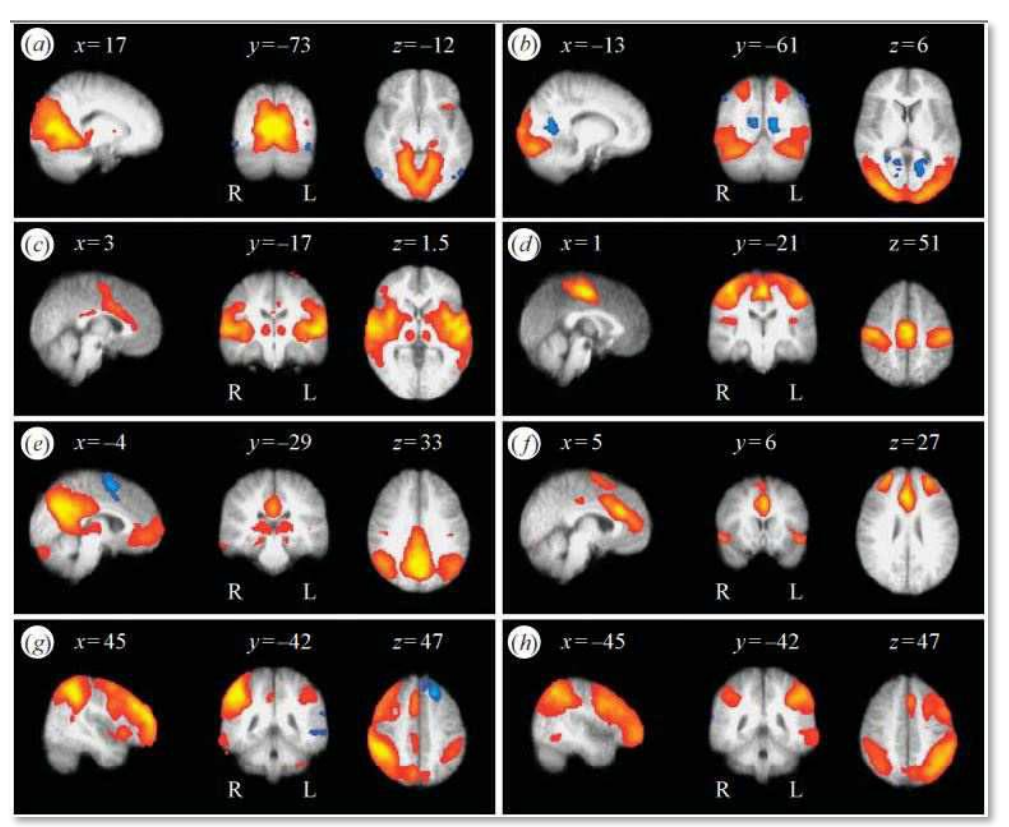
J. S. Damoiseaux<sup>+‡</sup>, S. A. R. B. Rombouts<sup>51</sup>, F. Barkhof<sup>1</sup>, P. Scheltens<sup>†</sup>, C. J. Stam<sup>††</sup>, S. M. Smith<sup>‡‡</sup>, and C. F. Beckmann<sup>‡‡</sup>

13848-13853 | PNAS | September 12, 2006 | vol. 103 | no. 37

www.pnas.org/cgi/doi/10.1073/pnas.0601417103



#### Dorsal attention network



(a)-(b) visual system

(c) auditory system, (d) sensorimotor system

(e) visuo-spatial system, (f) executive control

(g)-(h) dorsal visual stream

#### **Protocol and subjects:**

- Patients: N=13, 38.3  $\pm$  11.8 (6 M)

- Controls: N=13, 38.5  $\pm$  10.8 (6 M)

- Resting state GE-EPI (4:45 min)

Resting state GE-EPI (4:45 min)

Structural 3D MR image with high resolution (13 min)

NeuroImage: Clinical 17 (2018) 873-881

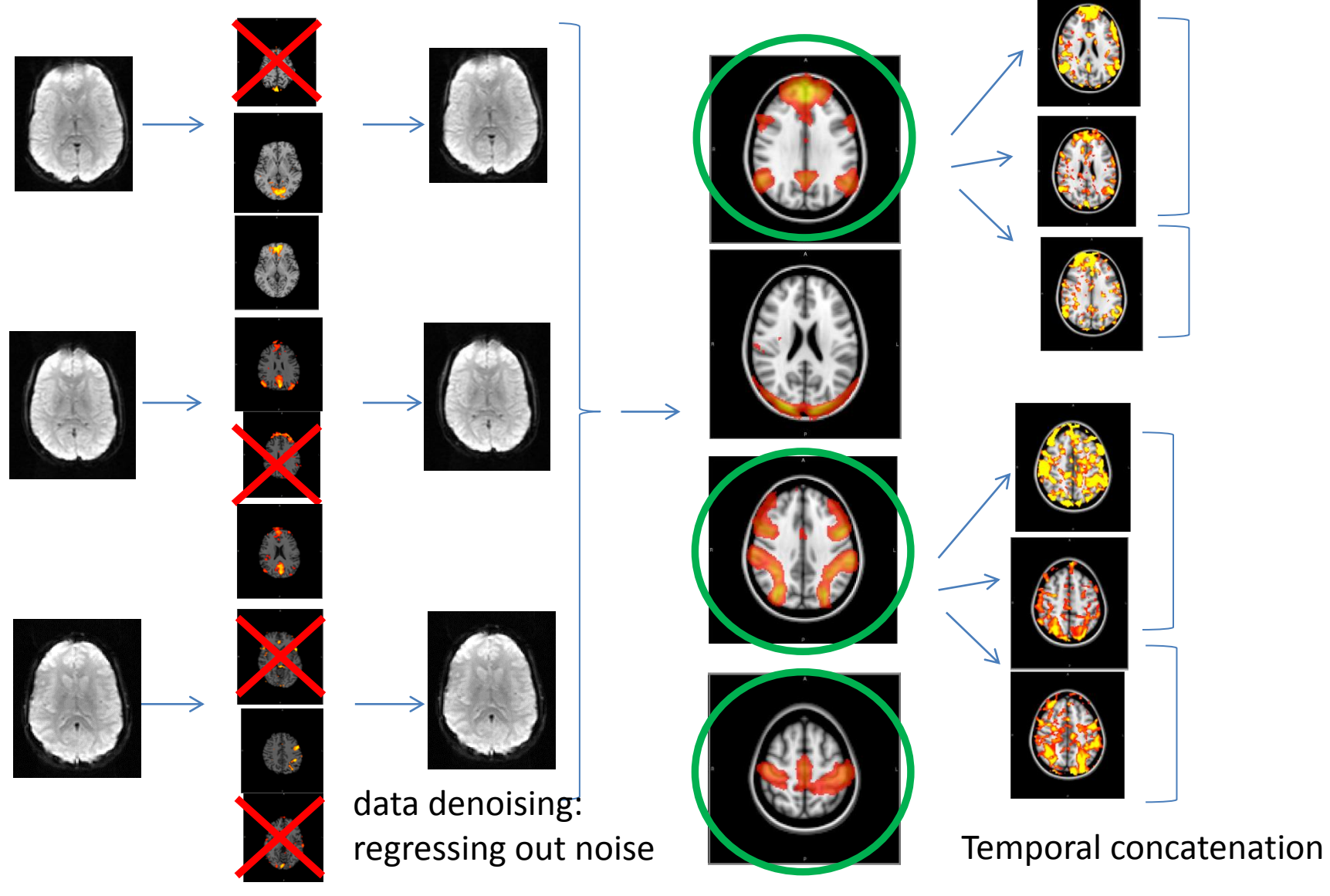
Contents lists available at ScienceDirect

NeuroImage: Clinical

journal homepage: www.elsevier.com/locate/ynicl

Brain functional connectivity in sleep-related hypermotor epilepsy

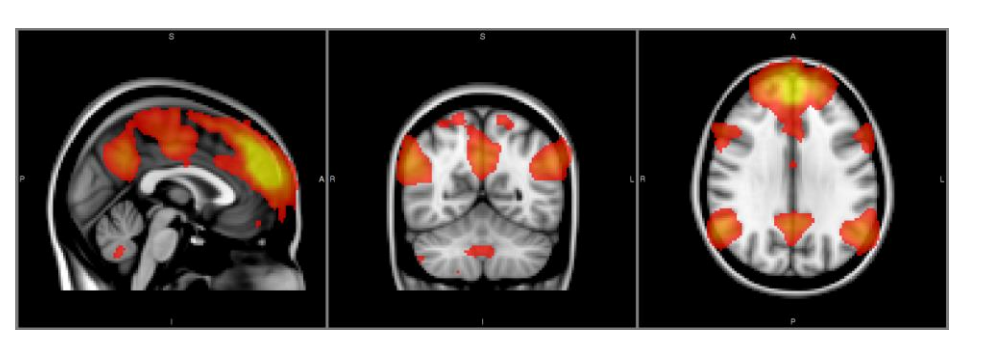
Stefania Evangelisti<sup>a,b,1</sup>, Claudia Testa<sup>a,b,c,1</sup>, Lorenzo Ferri<sup>b,d</sup>, Laura Ludovica Gramegna<sup>a,b</sup>, David Neil Manners<sup>a,b</sup>, Giovanni Rizzo<sup>b,d</sup>, Daniel Remondini<sup>c,e</sup>, Gastone Castellani<sup>c,e</sup>, Ilaria Naldi<sup>b,d</sup>, Francesca Bisulli<sup>b,d</sup>, Caterina Tonon<sup>a,b</sup>, Paolo Tinuper<sup>b,d</sup>, Raffaele Lodi<sup>a,b,\*</sup>



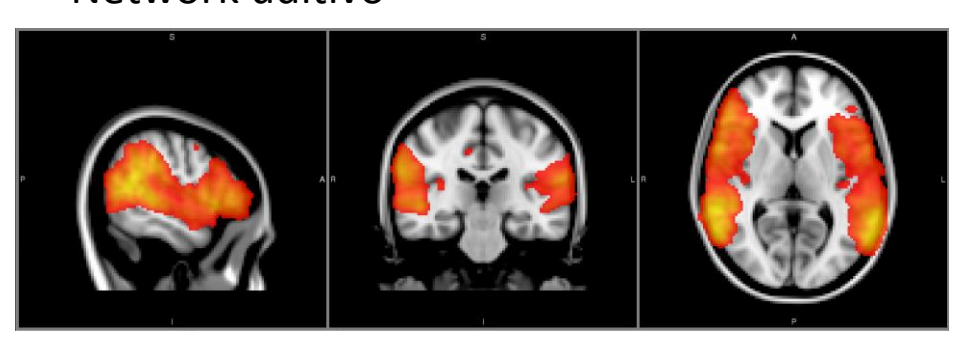
Classificazione: noise e signal

30 components: 16 noise componentes and 14 signal component

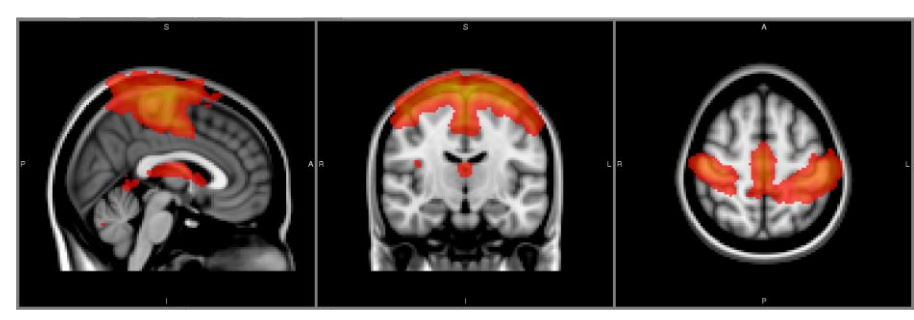
#### Default Mode Network



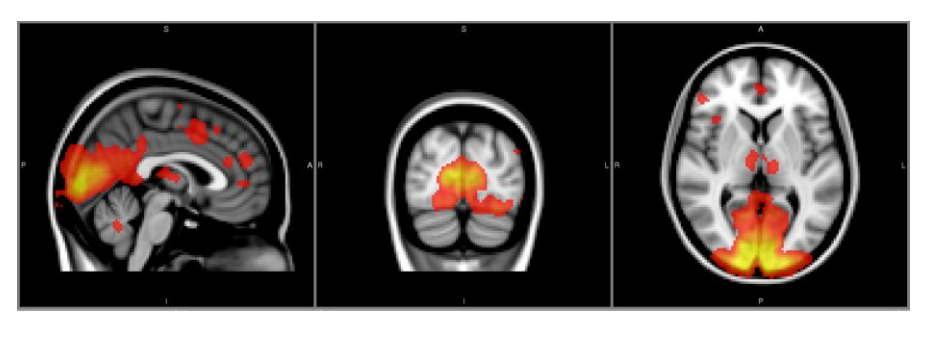
#### Network uditivo

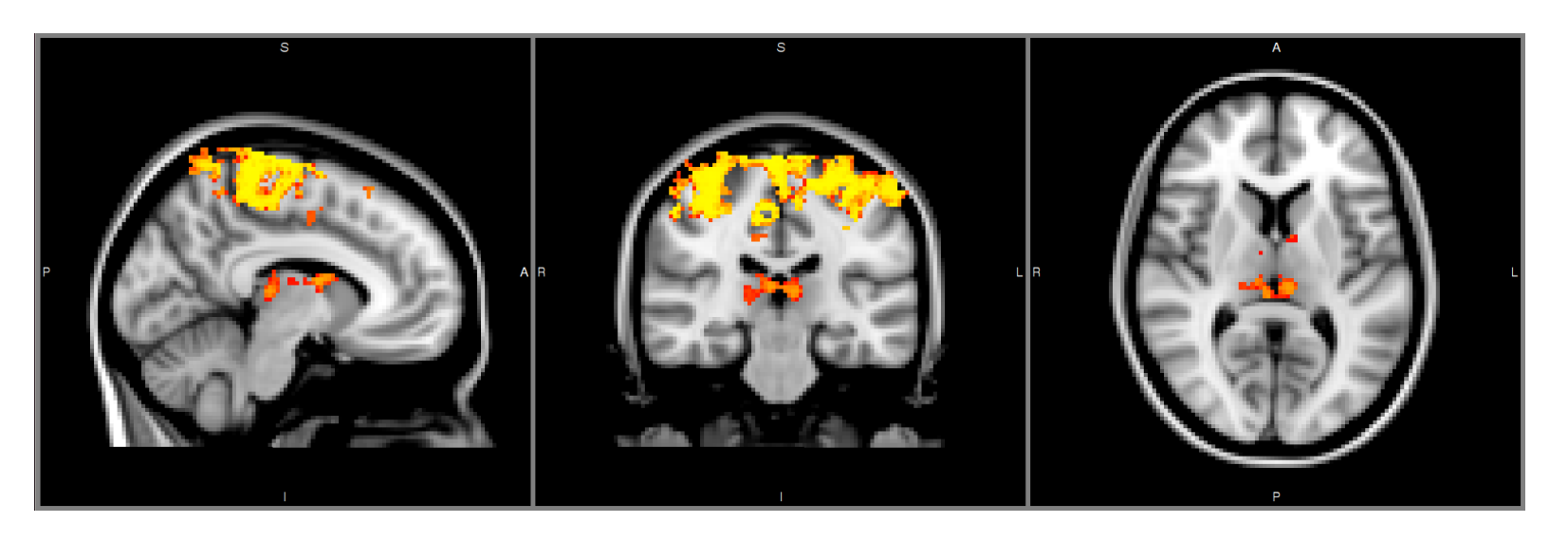


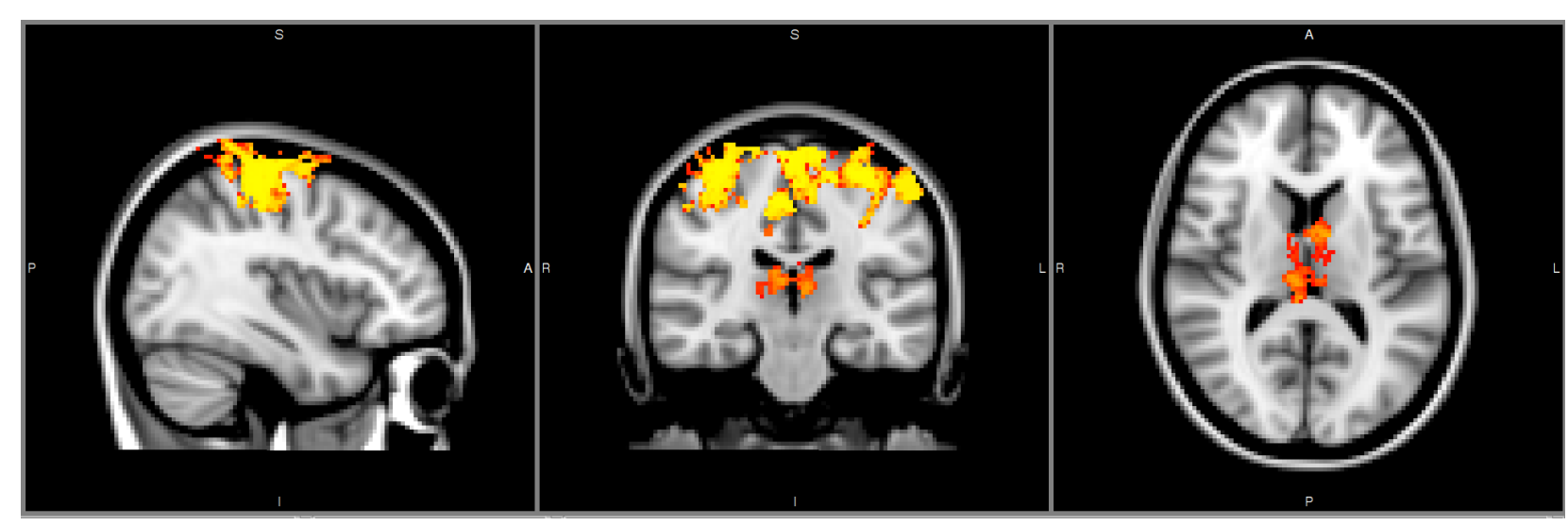
#### Network sensori-motorio



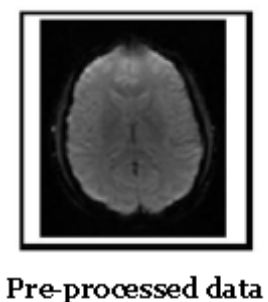
#### Network visivo







# Generation of the functional network: graph theory



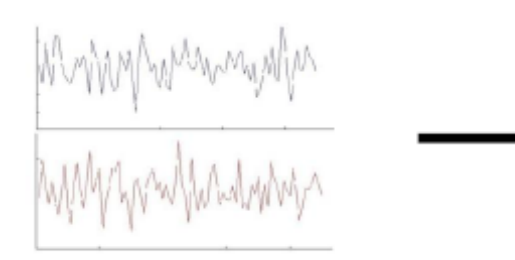


85 regions of interest (ROIs)

- .19 into deep grey matter
- .66 into cortex

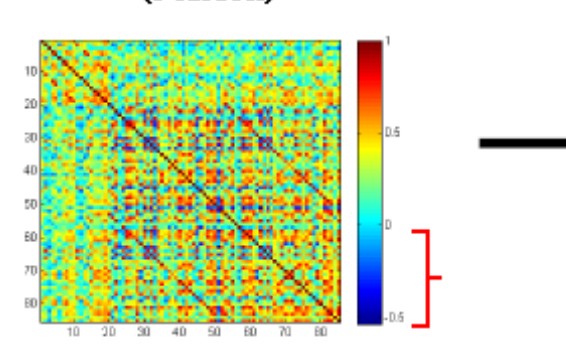
Nodes decision

Registration to 3D space

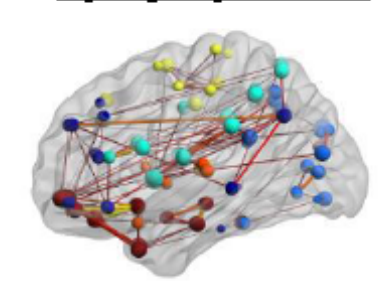


Time series exportation

Correlation analysis (Pearson)

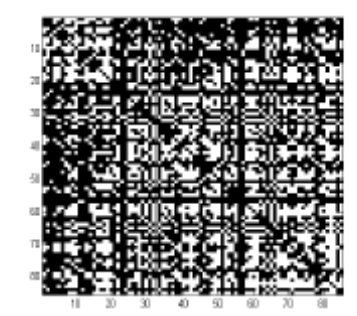


Brain network analysis using topological parameters

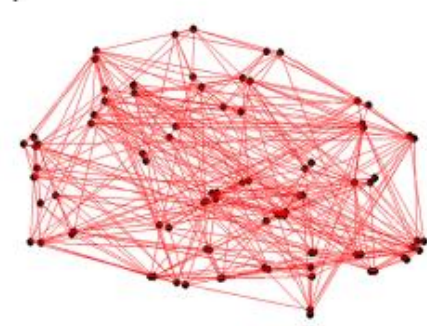




Thresholding







### Generation of the functional network: graph theory

## **Network specific measures:**

#### Global

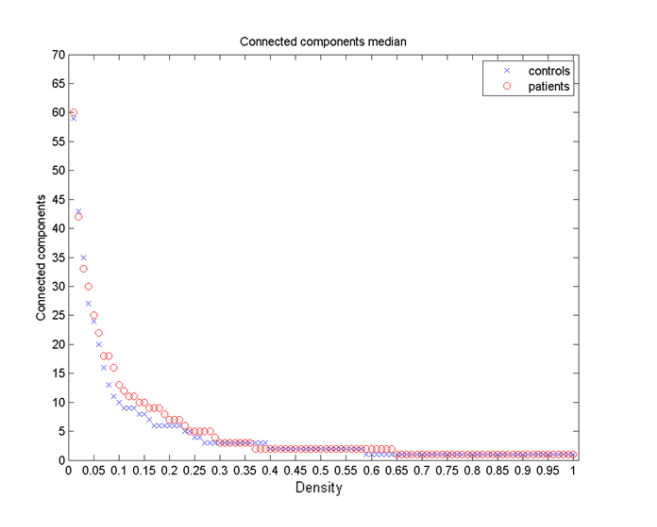
Connected components

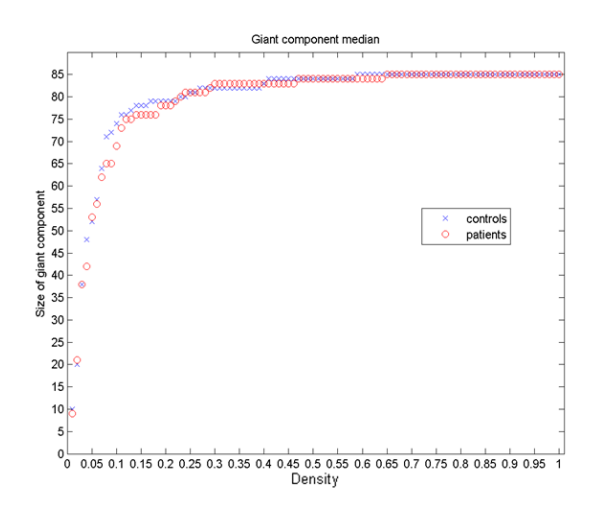
Small wordness (global efficiency and local efficiency)

#### Local

Node degree
Betweeness centrality
Clustering coefficient
Local efficiency

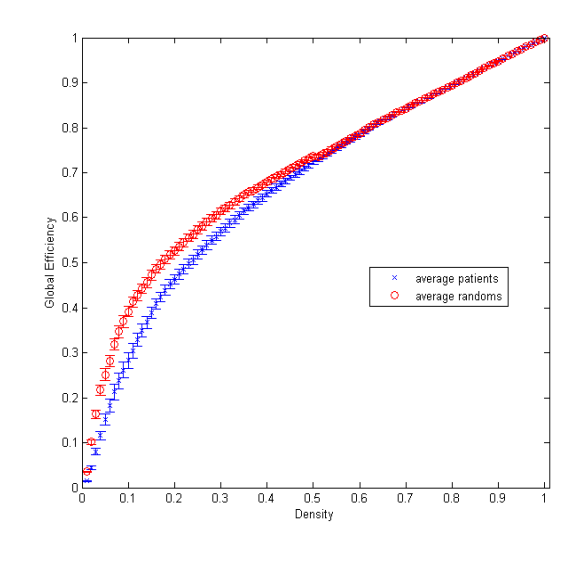
### **Connected components and giant component**

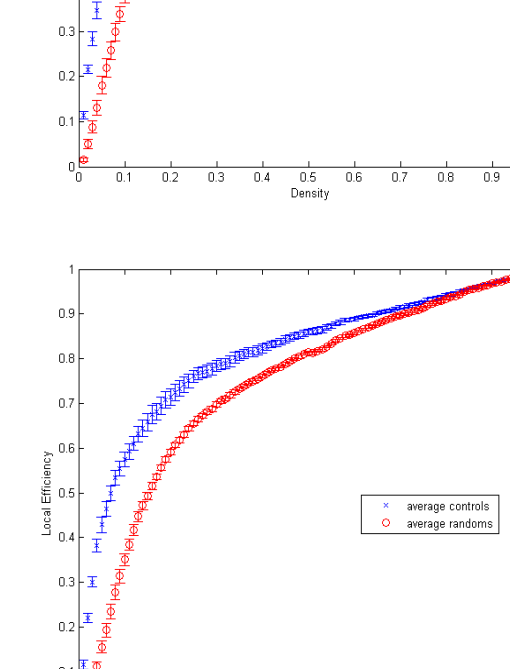




Plots of the number of connected components in the graphs (left) and of the dimension of the giant component over the whole range of densities (right). Median values among the two groups are reported, red dots represent patients and blue crosses represent healthy controls.

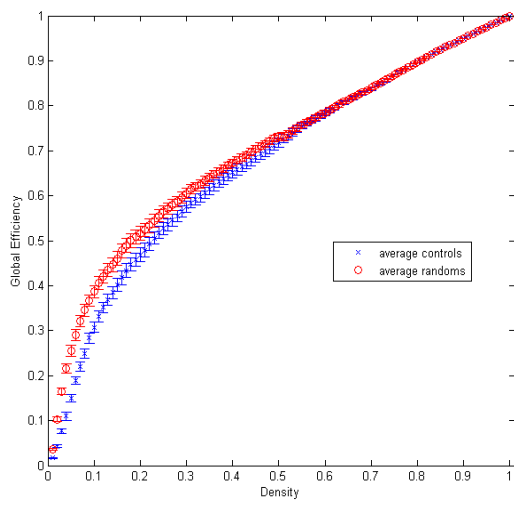
#### **Small wordness**





Density

ocal Effic



Results of small-word evaluation over the entire range of densities. Average values within random networks are shown in red, while average values within patients and controls are shown in blue. Top-left: comparison of global efficiency between patients and random network, top-right: comparison of local efficiency between patients and random network, bottom-left: comparison of global efficiency between controls and random network, bottom-right: comparison of local efficiency between control and random network.

#### **Local measures**

ND BCCC SHE > HC SHE < HC LE

Local measures were altered for SHE patients compared to healthy controls within the basal ganglia, limbic system, frontal lobe, visual cortex, parietal lobe, temporal lobe, brainstem and cerebellum

| Brain Region                 | ND       | BC       | CC | LE |
|------------------------------|----------|----------|----|----|
| Posterior cranial fossa      |          |          |    |    |
| Brainstem                    | -        | _        | 1  | 1  |
| Cerebellum cortex L          | <b>↓</b> | _        | _  | -  |
| Cerebellum cortex R          | <b>↓</b> | -        | -  | -  |
| Basal ganglia                |          |          |    |    |
| Caudate nucleus L            | -        | Į.       | 1  | 1  |
| Caudate nucleus R            | -        | -        | Ť  | 1  |
| Pallidum R                   | -        | -        | 1  | 1  |
| Frontal lobe                 |          |          |    |    |
| Caudal middle frontal R      | -        | Į.       | -  | -  |
| Lateral orbito frontal L     | -        | _        | 1  | -  |
| Lateral orbito frontal R     | -        | -        | 1  | -  |
| Pars opercularis R           | <b>†</b> | 1        | -  | -  |
| Pars triangularis L          | -        | 1        | -  | Į. |
| Pars triangularis R          | -        | 1        | -  | Į. |
| Precentral L                 | 1        | -        | -  | -  |
| Parietal lobe                |          |          |    |    |
| Superior parietal L          | <b>†</b> | <b>†</b> | _  | -  |
| Supramarginal L              | 1        | -        | -  | -  |
| Temporal lobe                |          |          |    |    |
| Fusiform R                   | <b>†</b> | _        | _  | -  |
| Transverse temporal          | -        | -        | Į. | Į. |
| Limbic system                |          |          |    |    |
| Amygdala L                   | <b>†</b> | †        | _  | -  |
| Amygdala R                   | -        | _        | _  | 1  |
| Insula R                     | <b>†</b> | 1        | -  | -  |
| Isthmus cingulate L          | -        | 1        | -  | -  |
| Isthmus cingulate R          | -        | 1        | -  | -  |
| Parahippocampal L            | -        | -        | Į. | Į. |
| Parahippocampal R            | -        | -        | -  | Į. |
| Posterior cingulate L        | -        | -        | 1  | 1  |
| Rostral anterior cingulate L | -        | -        | -  | Į. |
| Rostral anterior cingulate R | -        | -        | Į. | Į. |
| Visual system                |          |          |    |    |
| Cuneus R                     | -        | Į.       | †  | 1  |
| Lateral occipital L          | -        | Į.       | 1  | 1  |
| Pericalcarine L              | -        | Į.       | †  | 1  |
| Pericalcarine R              | -        | 1        | 1  | 1  |

# **Findings**

Dystonic-dyskinetic features suggest an involvement of basal ganglia (caudate, putamen and pallidum nuclei, substantia nigra and subthalamic nucleus)

Characteristic motor behaviors are sustained by ictal discharges that may originate in the frontal lobes (including **insula** and **anterior cingulate**) and in temporal lobe (including **amygdala**)

## Resting state fMRI: COVID olfactory disfunction

NeuroImage: Clinical 38 (2023) 103410



Contents lists available at ScienceDirect

NeuroImage: Clinical



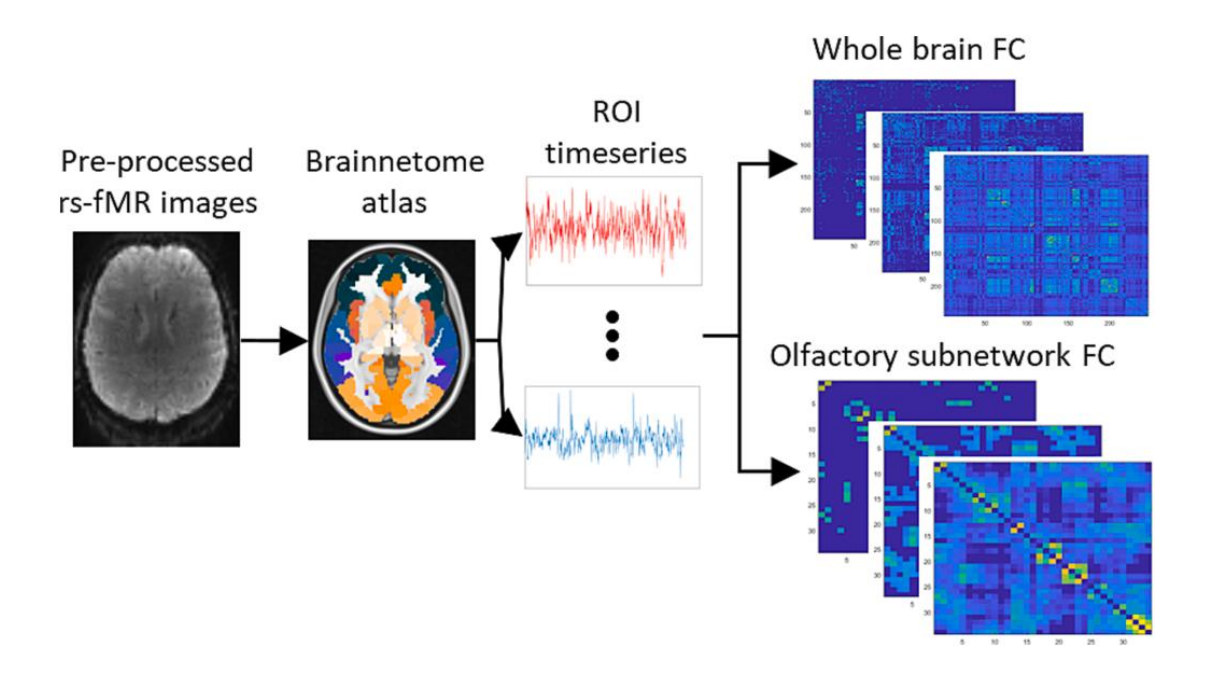




Cognitive and functional connectivity impairment in post-COVID-19 olfactory dysfunction

```
Lorenzo Muccioli <sup>a,1</sup>, Giovanni Sighinolfi <sup>a,1</sup>, Micaela Mitolo <sup>b,c</sup>, Lorenzo Ferri <sup>a</sup>, Magali Jane Rochat <sup>c</sup>, Umberto Pensato <sup>d</sup>, Lisa Taruffi <sup>a</sup>, Claudia Testa <sup>c,e</sup>, Marco Masullo <sup>a</sup>, Pietro Cortelli <sup>a,c</sup>, Raffaele Lodi <sup>a,c</sup>, Rocco Liguori <sup>a,c</sup>, Caterina Tonon <sup>a,c,2</sup>, Francesca Bisulli <sup>a,c,2,*</sup>
```

- Patients: N=23, 37 ± 14 (11 M) with persistent (≥1 month) OD with onset during COVID-19 infection, confirmed by an antigen or molecular-based test for SARS-CoV-2.
- Controls: N=26, 38  $\pm$  14 (13 M)
- 3T MR scanner equipped with a high-density head/neck array coil (64 channels). rs-fMRI (Gradient Echo Echo Planar Imaging, GRE-*EPI*, isotropic voxel 2.5x2.5x2.5 mm3, FOV 235 mm, repetition time TR = 735 ms, echo time TE = 37 ms, flip angle 53°, acquisition time 10 min).



Olfactory subnetwork: 13 bilateral cortex regions and 3 subcortical regions associated with the functional olfactory network:

Anterior cingulate cortex

5 sub-regions of the insula

4 sub-regions of the orbital cortex

**Rectus cortex** 

Parahippocampal cortex

Hippocampus

Amygdala

thalamus

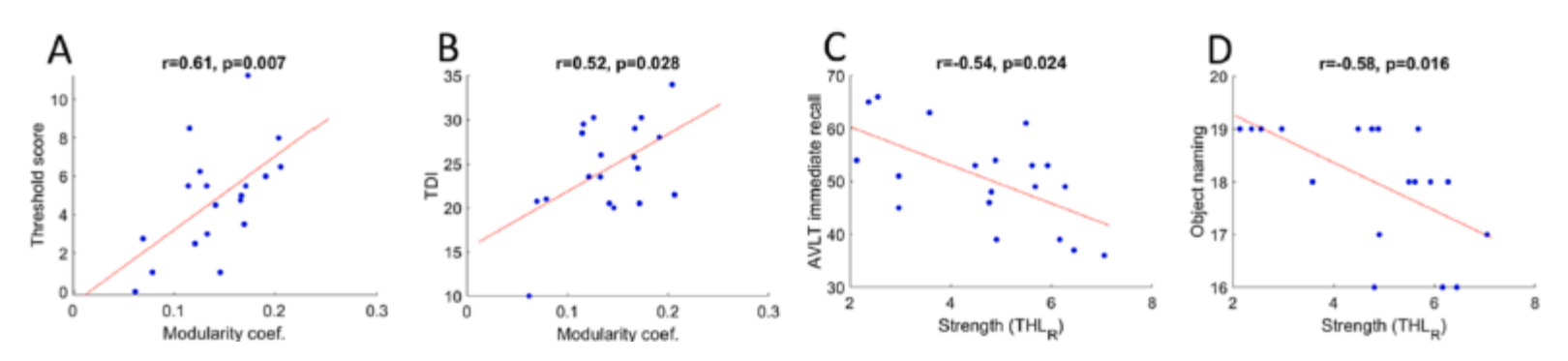
The morphometric analysis of the olfactory network did not show any significant alteration in patients compared to controls after correction for multiple comparisons.

No significant alterations emerged in the whole-brain graph analysis at the global level

Restricting the analysis to the olfactory sub-network, statistically significant alterations were detected both at the global and local levels in patients.

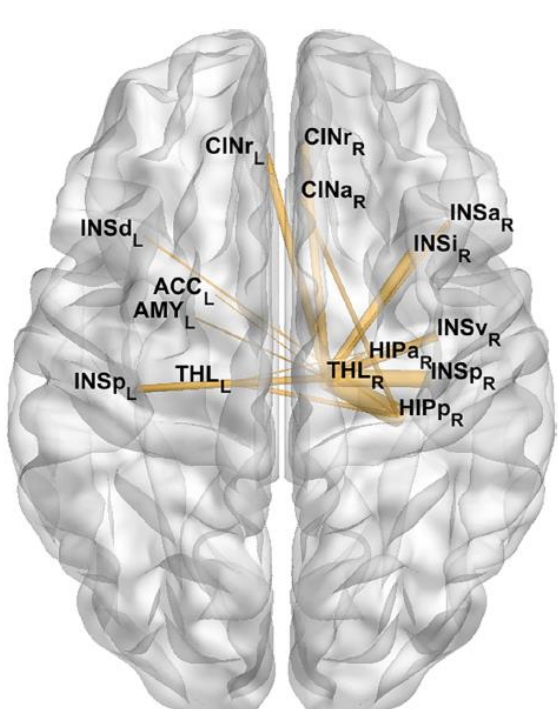
#### Global level in the olfactory sub-network.

The global modularity coefficient was significantly reduced in patients compared to controls (p = 0.03), indicating that long-COVID patients exhibited a sub-network structure with less closely segregated clusters than controls.

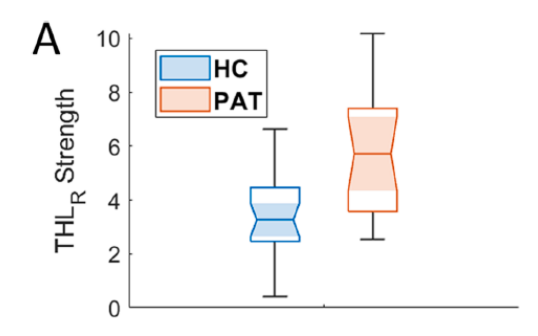


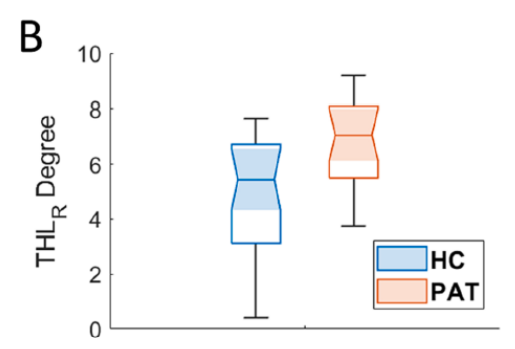
Results emerging from Pearson's correlations between the significantly altered functional graph properties of the olfactory network and the clinical scales. The modularity coefficient was found to have a significant positive relationship with the threshold (panel A) and the total scores (panel B) of the Sniffin' Sticks test, while the strength of the connections of the right thalamus showed a negative relation with short-term memory tests (panels C, D). AVLT, auditory verbal learning test; NPS, neuropsychological assessment

Local alterations of the centrality of the right thalamus were discovered, notably an increase of both the number (degree, p = 0.0008) and the strength (p = 0.0003) of the connections



Cluster of increased functional connectivity in patients within the olfactory network. The weights were assigned as the frequency over graph densities of the presence of altered connection, multiplied by the inverse p-value associated to the cluster at each density. The right thalamus constituted the center of this cluster, and its links with the right posterior hippocampus and insula were the most significantly altered.





Boxplot of strength (panel A) and degree (panel B) of the right thalamus in patients (red) and controls (light blue). The two quantities differed significantly between the two groups. HC, healthy controls; PAT, long-COVID; THLR, right thalamus.

# Thank you for your attention!

Chiara Malvaso – PhD student

Maddalena Cavallo - PhD student



Carlo Golini - PhD student

Leonardo Brizi – Senior Assitant Professor



Mattia Ricchi - PhD student

**NMR Laboratory** 

**Department of Physics and Astronomy University of Bologna**